

Interference Management by Harnessing Multi-Domain Resources in Spectrum-Sharing Aided Satellite-Ground Integrated Networks

Xiaojin Ding, *Member, IEEE*, Yue Lei, Yulong Zou, *Senior Member, IEEE*, Gengxin Zhang, *Member, IEEE* and Lajos Hanzo, *Life Fellow, IEEE*

Abstract—A spectrum-sharing satellite-ground integrated network is conceived, consisting of a pair of non-geostationary orbit (NGSO) constellations and multiple terrestrial base stations, which impose the co-frequency interference (CFI) on each other. The CFI may increase upon increasing the number of satellites. To manage the potentially severe interference, we propose to rely on joint multi-domain resource aided interference management (JMDR-IM). Specifically, the coverage overlap of the constellations considered is analyzed. Then, multi-domain resources - including both the beam-domain and power-domain - are jointly utilized for managing the CFI in an overlapping coverage region. This joint resource utilization is performed by relying on our specifically designed beam-shut-off and switching based beam scheduling, as well as on long short-term memory based joint autoregressive moving average assisted deep Q network aided power scheduling. Moreover, the outage probability (OP) of the proposed JMDR-IM scheme is derived, and the asymptotic analysis of the OP is also provided. Our performance evaluations demonstrate the superiority of the proposed JMDR-IM scheme in terms of its increased throughput and reduced OP.

Index Terms—Multi-domain resources allocation, non-geostationary orbit constellation, outage probability, spectrum sharing, space-ground integrated network.

I. INTRODUCTION

LOW-Earth-Orbit (LEO) satellites have the potential of extending the coverage of terrestrial networks, while maintaining a low propagation delay [1]. Moreover, deploying base stations onboard of LEO satellites is capable of promptly setting up a networking infrastructure even in natural disaster areas. Thus, LEO satellites have attracted extensive research attention all over the world. Numerous LEO constellations have been proposed, as exemplified by Telesat [2], Starlink [3], and OneWeb [4]. These constellations are capable of simultaneously providing multiple LEO satellite links for

a single user [5], [6]. Therefore, the power constraint of conventional small constellations can be readily overcome, since the required power can be jointly provided by multiple satellites. However, multiple satellites simultaneously occupy the spectral resources of a constellation, hence reducing the spectral efficiency.

Recently, sophisticated spectrum sharing techniques have emerged as an effective means of addressing the spectrum scarcity problem [7]. The most popular spectrum sharing modes are the overlay [8] and the underlay mode [9]. *In the overlay mode*, spectrum sharing is performed with the aid of accurate spectrum sensing and spectrum prediction both in integrated satellite-terrestrial networks [8], [10], as well as in integrated geostationary (GEO) and nongeostationary (NGSO) scenarios [11]. Since spectrum sensing may fail to work reliably, the potential blind spots of spectrum sensing were explored for assisting spectrum sharing between GEO and NGSO scenarios in [12]. These overlay based spectrum-sharing schemes beneficially exploit the existence of the spectrum holes. By contrast, spectrum sharing may also be exploited even in the absence of spectrum holes with the aid of the underlay mode, albeit at the cost of incurring co-frequency interference [13], which has to be managed. *Hence the underlay mode tends to require a combination of the following interference-management techniques*: accurate power control [14], frequency hopping [15], sophisticated channel selection [16], some frequency-reuse planning [17], and refined beam control [18]. Specifically, a pair of optimal power control schemes were designed for a LEO satellite constellation in support of coexistence with terrestrial networks in [14]. Frequency hopping was used for spectrum sharing between fixed satellite services and tactical data links in [15]. As a further advance, a game-theory aided channel selection method was designed to meet the access requirements of primary and secondary users in [16]. To perform spectrum sharing for both cellular, as well as NGSO and GEO systems, the required geographic protection/exclusion-zone of frequency reuse was calculated in [17]. Furthermore, adaptive beam control was proposed for managing the interference imposed on the terrestrial networks by satellites [18].

In contrast to the aforementioned single-dimensional spectrum-sharing schemes used in the overlay mode, multi-dimensional scheduling aided spectrum sharing schemes have also been designed for alleviating the co-frequency interference (CFI) [19]–[21]. A joint resource allocation algorithm

This work presented was partially supported by the National Science Foundation of China (No. 62171234, 91738201), the Jiangsu Province Basic Research Project (No. BK20192002), and the China Postdoctoral Science Foundation (No. 2018M632347).

Xiaojin Ding, Yue Lei, Yulong Zou and Gengxin Zhang are with the Telecommunication and Networks National Engineering Research Center, Nanjing University of Posts and Telecommunications, Nanjing 210003, China. E-mail: {dxj, 1022072005, yulong.zou, zgx}@njupt.edu.cn.

L. Hanzo is with the Department of Electronics and Computer Science, University of Southampton, Southampton, United Kingdom. (E-mail: lh@ecs.soton.ac.uk)

L. Hanzo would like to acknowledge the financial support of the Engineering and Physical Sciences Research Council projects EP/W016605/1, EP/X01228X/1 and EP/Y026721/1 as well as of the European Research Council's Advanced Fellow Grant QuantCom (Grant No. 789028)

was designed for increasing the throughput [19] by considering the interbeam interference, as well as the bandwidth allocation and power allocation. Moreover, sophisticated user association, bandwidth assignment and power allocation were jointly used for spectrum sharing in a terrestrial-satellite network [20]. As a further development, a joint beamforming and power allocation scheme was designed for allowing a satellite network to share its spectrum with a terrestrial network [21]. For a coexisting LEO and GEO satellite system, a joint power allocation supported by tight cooperation amongst the LEO satellites was proposed for managing the interference imposed on GEO users by the LEO satellites.

Whilst extensive efforts have been invested in supporting the coexistence of GEO, LEO and terrestrial wireless networks (CGLT), less attention has been dedicated to satellite-ground integrated networks (SGIN) relying on multiple NGSO constellations and terrestrial systems. In contrast to the CGLT scenarios, spectrum-sharing aided NGSO constellations travel at speed, hence resulting in violently time-varying interference. Moreover, NGSO constellations in each other's vicinity may impose severe CFI on each other's receivers in the presence of spectrum sharing, which may be classified into intra-constellation and inter-constellation (system) interference. Compared to the inter-constellation CFI, it is less challenging to manage the intra-constellation CFI, since the owner has the ability to configure its constellation [22]. To avoid the inter-constellation CFI, the inter-system interference of NGSO constellations in coexistence with GEO systems was analyzed in [22], and the efficiency of low-complexity interference management schemes was also evaluated. However, the performance evaluations in [22] indicated that the existing spectrum regulation schemes may be unable to guarantee the target-reliability of the system analyzed. Moreover, the interference scenario of NGSO satellite communication systems was analyzed, and the challenges of alleviating the CFI between NGSO constellations were investigated in [23].

Against the above backdrop, we conceive inter-system interference management techniques for spectrum-sharing aided SGIN, including a pair NGSO constellations and multiple terrestrial base stations (BSs). Explicitly, one of the NGSO constellations, namely NGSO 1, shares its spectrum both with the other constellation, denoted by NGSO 2, and with the BSs. Our interference analysis indicates the existence of severe CFI. To manage the CFI caused by spectrum sharing, an optimization problem is formulated for maximizing the throughput of NGSO 1, whilst still meeting the transmission requirements of both NGSO 2 and of the BSs. However, it is challenging to directly solve this complex problem, since it depends on numerous factors, such as the coverage overlap of NGSO constellations, the transmit power, on the number of satellites available, the tele-traffic model, the channel state information (CSI) and on the transmission requirements. Thus, this excessively complex problem is decoupled. Specifically, we first analyze the coverage overlap between NGSO 1 and NGSO 2. To further manage the CFI, the beam-domain and power-domain resources are jointly scheduled for solving the optimization problem formulated. Additionally, the outage probability of the associated wireless-transmission links is also evaluated.

The main contributions of this paper are boldly contrasted to the literature in Table I for visualizing the knowledge-gaps. Overall, in contrast to [4], [12], [14], [17], [18], [20], [21], the effects of both the inter-constellation CFI and of the intra-constellation CFI are analyzed in this paper. To mitigate the effect of the inter-constellation CFI, multi-domain resources - including both the beam-domain and power-domain - are used for meeting the stringent requirements of a spectrum-sharing SGIN. We characterized them with the aid of their coverage analysis and their predicted CSI. Moreover, their closed-form outage probability (OP) and asymptotic OP (AOP) expressions were derived to assist in evaluating the overall performance of our proposed scheme. The main contributions of this paper are summarized as follows.

Firstly, we propose joint multi-domain resource aided interference management (JMDR-IM) for a SGIN, relying on analyzing the coverage overlap, and on beneficially scheduling both the beam-domain and power-domain resources. Specifically, the coverage overlap is analyzed for identifying the potentially interfering satellites, and the alternative satellites available for substituting these interfering satellites. The equations derived may be beneficially used for designing a variety of similar systems. Moreover, the concept of co-frequency exclusion zone (CFEZ) is conceived.

Secondly, the activation of the beam-domain and power-domain resources is harmonized for managing the CFI by relying on our coverage overlap expressions. Specifically, the beam-domain scheduling based on the shutting off and switching beams is adopted for eliminating the CFI. Following the beam-domain scheduling issues, we conceive a long short-term memory based joint autoregressive moving average and deep Q network (LSTM-ARMA-DQN) aided power allocation scheme. Explicitly, this LSTM-ARMA-DQN scheme combines the LSTM-ARMA and the DQN philosophies, where the LSTM-ARMA is used for predicting the CSI of the satellite links, while the DQN is harnessed for optimizing the transmit power of our SGIN.

Thirdly, we present the OP and the AOP analysis of the proposed JMDR-IM scheme. Closed-form expressions are derived for the SGIN considered. Moreover, the asymptotic analysis of the OP and the AOP are also provided for further evaluating the performance of the proposed JMDR-IM scheme, and for verifying the accuracy of the OP and the AOP expressions derived.

Finally, we show that the proposed JMDR-IM scheme achieves a higher throughput despite its lower OP than that of the conventional pure stand-alone power allocation using fixed beams (PPAFB). Furthermore, the proposed JMDR-IM scheme maintains a high signal-to-interference plus noise ratio (SINR), which is achieved through tracking the dynamically fluctuating CFI of a SGIN.

The remainder of the paper is as follows. In Section II, we briefly present our system model, coverage analysis and the co-frequency exclusion zone concept. In Section III, we propose the JMDR-IM scheme, including our beam shut-off and beam-switching based scheduling, as well as the LSTM-ARMA-DQN based power allocation. In Section IV, we derive the OP of the proposed JMDR-IM scheme, while in Section

TABLE I
BOLDLY CONTRASTING OUR NOVELTY TO THE EXISTING LITERATURE

	[4]	[12]	[14]	[17]	[18]	[20]	[21]	Our Work
Spectrum sharing	✓	✓	✓	✓	✓	✓	✓	✓
Among satellites (e.g., GEO and LEO, LEO and LEO)	✓	✓						✓
Satellites in coexistence with terrestrial systems			✓	✓	✓	✓		✓
SGIN including GEO, LEO and terrestrial systems				✓				✓
Coverage analysis								✓
Power control			✓			✓	✓	✓
Beam control	✓				✓		✓	✓
Deep learning and CSI prediction aided resource scheduling								✓
Outage probability analysis			✓	✓				✓
Asymptotic outage probability analysis								✓

V we conclude. The main variables and symbols used in this paper is listed in Table II for easy reference.

TABLE II
VARIABLE AND SYMBOLS LIST

Notation	Definition
NGSO 1, NGSO 2	NGSO constellations
N_{1n}, N_{2m}	NGSO satellites
BS_i, BS_z	Terrestrial base station (BS)
$p(N_{1n}), p(N_{2m})$ and $p(BS_i)$	Locations of the NGSO satellites, and of the terrestrial BS
$p(U_{N_1}^k), p(U_{N_2}^j)$, and $p(U_{BS}^t)$	Locations of users for the NGSO satellites, and of users for the terrestrial BS
$U_{N_1}^k, U_{N_2}^j$ and U_{BS}^t	Users of satellites and BSs
$\{l_{N_{1n}}^a, l_{N_{1n}}^o\}, \{l_{U_{N_1}^k}^a, l_{U_{N_1}^k}^o\}, \{l_{N_{2m}}^a, l_{N_{2m}}^o\}, \{l_{U_{N_2}^j}^a, l_{U_{N_2}^j}^o\}, \{l_{BS_i}^a, l_{BS_i}^o\}, \{l_{U_{BS}^t}^a, l_{U_{BS}^t}^o\}$	Latitude and longitude
$P_n, P_m, P_i, P_z, P_n^o, P_m^o, P_i^o, P_z^o$	Transmit power
$h_{nk}, h_{mk}, h_{ik}, h_{mj}, h_{nj}, h_{ij}, h_{it}, h_{zt}, h_{nt}, h_{mt}$	Instantaneous CSI
$L_{nk}^S, L_{mk}^S, L_{ik}^S, L_{mj}^S, L_{nj}^S, L_{ij}^S, L_{it}^S, L_{zt}^S, L_{nt}^S, L_{mt}^S$	Free-space loss
$G_{nU_{N_1}^k}^t, G_{mU_{N_1}^k}^r, G_{mU_{N_1}^k}^t, G_{nU_{N_2}^j}^t, G_{rU_{N_2}^j}^r, G_{mU_{N_2}^j}^r, G_{nU_{N_2}^j}^t, G_{rU_{N_2}^j}^t, G_{mU_{N_2}^j}^t, G_{mU_{BS}^t}^t$	Antenna gain
$x_{N_1}^n, x_{N_2}^m, x_{BS}^i, x_{BS}^z$	Transmitted signals
α_m, α_n	Traffic states
n_k, n_j, n_t	Gaussian noise
$N_{S1}, N_{S2}, N_{S3}, N_{S4}, N'_{S1}, N'_{S2}, N'_{S3}, N'_{S4}$	The number of interfering satellites
$b_{N_{1n}}^i$	Satellites' beams
$\Phi_{N_{2m} \rightarrow U_{N_1}^k}, \Phi_{N_{2m} \rightarrow U_{N_2}^j}, \Phi_{N_{2m} \rightarrow U_{BS}^t}, \Phi_{N_{1n} \rightarrow U_{N_1}^k}, \Phi_{N_{1n} \rightarrow U_{N_2}^j}, \Phi_{N_{1n} \rightarrow U_{BS}^t}$	Satellites' sets of covering users
$P_{NGSO1}^{\max}, P_{NGSO2}^{\max}, P_{BS}^{\max}$	Maximum available transmit power
LEO, GEO	Low-Earth-Orbit, Geostationary
NGSO	Nongeostationary
SGIN	Satellite-ground integrated network
CFI, CSI	Co-frequency interference, Channel state information
CFEZ	Co-frequency exclusion zone
JMDR-IM	Joint multi-domain resource aided interference management
LSTM-ARMA-DQN	Long short-term memory based joint autoregressive moving average and deep Q network
PPAFB	Pure stand-alone power allocation using fixed beams
OP, AOP	Outage probability, Asymptotic outage probability
SINR	Signal-to-interference plus noise ratio

II. SYSTEM MODEL AND COVERAGE ANALYSIS

A. System Model

As shown in Fig. 1, we investigate a spectrum-sharing SGIN, composed of two LEO constellations, represented by N_{1n} and N_{2m} , and multiple terrestrial BSs, denoted by BS_i , where $1 \leq n \leq N$, $1 \leq m \leq M$, $1 \leq i \leq N_B$. Explicitly, N , M and N_B are the number of NGSO 1 satellites, of NGSO 2 satellites and of the BSs, respectively. Moreover, their users are denoted by $U_{N_1}^k, U_{N_2}^j$ and U_{BS}^t , where $1 \leq k \leq K$, $1 \leq j \leq J$ and $1 \leq t \leq N_t$. Furthermore, K , J and N_t are the number of users of the NGSO 1, of the NGSO 2 and of the BSs, respectively. The location of each satellite is represented by the latitude and the longitude. Thus, given the n -th satellite of NGSO 1 and the k -th user, their locations are $p(N_{1n}) = \{l_{N_{1n}}^a, l_{N_{1n}}^o\}$ and $p(U_{N_1}^k) = \{l_{U_{N_1}^k}^a, l_{U_{N_1}^k}^o\}$. Similarly, given the m -th satellite of NGSO 2 and the j -th user, their locations are $p(N_{2m}) = \{l_{N_{2m}}^a, l_{N_{2m}}^o\}$ and $p(U_{N_2}^j) = \{l_{U_{N_2}^j}^a, l_{U_{N_2}^j}^o\}$. Let $p(BS_i) = \{l_{BS_i}^a, l_{BS_i}^o\}$ and $p(U_{BS}^t) = \{l_{U_{BS}^t}^a, l_{U_{BS}^t}^o\}$ denote the locations of the i -th BS and its t -th user, respectively. We also assume that the channel spanning from any satellite to any user is accurately represented by a Shadowed-Rician fading model [24]. Moreover, we use a Rayleigh fading channel for modeling all the links between any BS and any user. We also use a Poisson model for characterizing the tele-traffic of both NGSO 1 and NGSO 2 [25]. Furthermore, we consider a scenario, where NGSO 1 and NGSO 2 occupy two different orbits, and they are equipped with switchable multi-beam antennas capable of pointing in specific directions [26].

As shown in Fig. 1, we assume that the multi-color multi-beam frequency-reuse scheme is employed by both NGSO 1 and NGSO 2. For notational convenience, we consider single-color beams for representing all multi-color beams as an example, but all remaining beams can be expressed similarly. We assume that given the n -th satellite, a beam of this satellite transmits its signal to the k -th user of NGSO 1, thus the signal received at $U_{N_1}^k$ is given by

$$y_{U_{N_1}^k} = \sqrt{P_n} G_{nU_{N_1}^k}^t G_{mU_{N_1}^k}^r L_{nk}^S h_{nk} x_{N_1}^n + \sum_{i \in \Phi_{BS}} \sqrt{P_i} L_{ik}^S h_{ik} x_{BS}^i + \sum_{m=1}^{N_{S1}} \sqrt{\alpha_m P_m} G_{mU_{N_1}^k}^t G_{rU_{N_1}^k}^r L_{mk}^S h_{mk} x_{N_2}^m + n_k, \quad (1)$$

where P_n, P_m and P_i denote the transmit power of N_{1n}, N_{2m} and BS_i , respectively. Furthermore, $x_{N_1}^n, x_{N_2}^m$ and x_{BS}^i

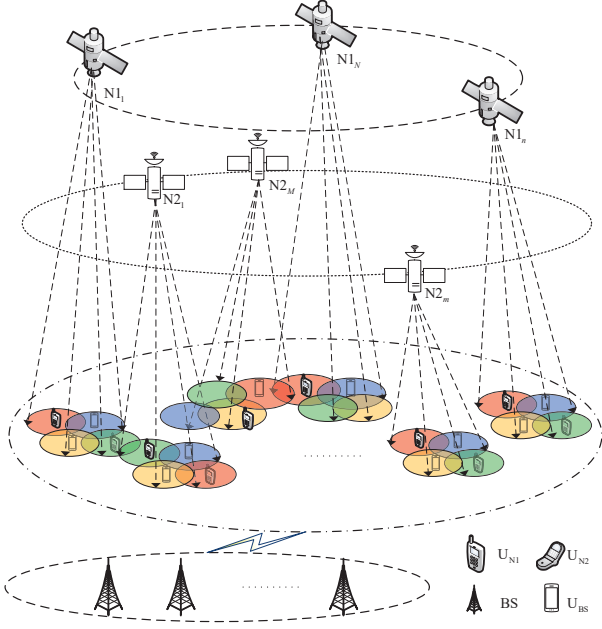


Fig. 1. A spectrum-sharing SGIN, including a pair of NGSO constellations and multiple terrestrial BSs.

respectively denote the random symbols transmitted by the n -th satellite of NGSO 1, the m -th satellite of NGSO 2 and the i -th BS of the BS set. We also assume $E[|x_{N1}^n|^2] = E[|x_{N2}^m|^2] = E[|x_{BS}^i|^2] = 1$, where $E[\cdot]$ represents the expected value. The variable N_{S1} represents the number of satellites imposing interference on U_{N1}^k , while n_k is the zero-mean noise received at U_{N1}^k having a variance of $k_B B_n T_n$, with k_B , B_n and T_n denoting the Boltzmann constant, the transmission bandwidth of $N1_n$'s beam and the equivalent noise temperature, respectively. The variables h_{nk} , h_{mk} and h_{ik} denote the instantaneous CSI of the links spanning from $N1_n$ to U_{N1}^k , from $N2_m$ to U_{N1}^k and from BS_i to U_{N1}^k , respectively. Additionally, L_{nk}^S , L_{mk}^S and L_{ik}^S represent the free-space loss of the $N1_n$ - U_{N1}^k , $N2_m$ - U_{N1}^k and BS_i - U_{N1}^k links [40], while α_m represents the traffic state of $N2_m$'s beam, where the traffic state is assumed to obey the Poisson distribution [25]. If there is no tele-traffic during a given transmission slot, we have $\alpha_m = 0$. Otherwise, we have $\alpha_m = 1$. Furthermore, G_{ab}^d denotes the antenna gain of the satellites and their users, and we have $G_{ab}^d = G_0 \left[\frac{J_1(\mu)}{2\mu} + 36 \frac{J_3(\mu)}{\mu^3} \right]^2$ [21], where $\mu = 2.07123 \sin(\theta) / \sin(\theta_{3dB})$, θ and θ_{3dB} respectively represent the off-boresight angle and the 3 dB angle. In this antenna-gain expression, J_1 and J_3 denote the Bessel functions of the first order and the third order, respectively, while $G_0 = \xi \left(\frac{\pi D_e}{c/f} \right)^2$, D_e , c , f and ξ respectively denote the antenna diameter, the light velocity, the frequency band and the antenna efficiency. Finally, $a \in \{n, m\}$, $b \in \{U_{N2}^j, U_{N1}^k\}$, $d \in \{t, r\}$ and $e \in \{N1_n, N2_m, U_{N1k}, U_{N2j}\}$.

Similarly, given the m -th NGSO 2 satellite and the j -th

NGSO 2 user, the signal received at U_{N2}^j is formulated as

$$y_{U_{N2}^j} = \sqrt{P_m G_{mU_{N2}^j}^t G_{mU_{N2}^j}^r L_{m_j}^S} h_{m_j} x_{N2}^m + \sum_{i \in \Phi_{BS}} \sqrt{P_i L_{ij}^S} h_{ij} x_{BS}^i + \sum_{n=1}^{N_{S2}} \sqrt{\alpha_n P_n G_{nU_{N2}^j}^t G_{nU_{N2}^j}^r L_{n_j}^S} h_{n_j} x_{N1}^n + n_j, \quad (2)$$

where N_{S2} is the number of satellites imposing interference on U_{N2}^j . In (2), n_j is the noise received at U_{N2}^j having a zero mean and a variance of $k_B B_m T_n$, B_m is the transmission bandwidth of $N2_m$'s beam. Furthermore, h_{m_j} , h_{n_j} and h_{ij} represent the CSIs of the links from $N2_m$ to U_{N2}^j , from $N1_n$ to U_{N2}^j and from BS_i to U_{N2}^j , respectively. Still referring to (2), $L_{m_j}^S$, $L_{n_j}^S$ and L_{ij}^S represent the free-space loss of the $N2_m$ - U_{N2}^j , $N1_n$ - U_{N2}^j and BS_i - U_{N2}^j links. Similarly to α_m , α_n denotes the traffic state of $N1_n$'s beam, and we have $\alpha_n \in \{0, 1\}$.

To elaborate further, the signal received at U_{BS}^t and transmitted by BS_i is written as

$$y_{U_{BS}^t} = \sqrt{P_i L_{it}^S} h_{it} x_{BS}^i + \sum_{n=1}^{N_{S3}} \sqrt{\alpha_n P_n G_{nU_{BS}^t}^t L_{nt}^S} h_{nt} x_{N1}^n + \sum_{m=1}^{N_{S4}} \sqrt{\alpha_m P_m G_{mU_{BS}^t}^t L_{mt}^S} h_{mt} x_{N2}^m + \sum_{z \in \Phi_{BS}, z \neq i} \sqrt{P_z L_{zt}^S} h_{zt} x_{BS}^z + n_t, \quad (3)$$

where N_{S3} and N_{S4} respectively denote the number of NGSO 1 satellites and NGSO 2 satellites imposing interference on U_{BS}^t . Furthermore, n_t is the noise received at U_{BS}^t having a zero mean and a variance of σ_n^2 . In (3), h_{it} , h_{zt} , h_{nt} and h_{mt} represent the CSIs of the links spanning from BS_i to U_{BS}^t , from BS_z to U_{BS}^t , from $N1_n$ to U_{BS}^t and from $N2_m$ to U_{BS}^t , respectively. Moreover, L_{it}^S , L_{zt}^S , L_{nt}^S and L_{mt}^S represent the free-space loss of the BS_i - U_{BS}^t , BS_z - U_{BS}^t , $N1_n$ - U_{BS}^t and $N2_m$ - U_{BS}^t links, respectively. Moreover, in (3), the inter-cell CFI is considered [37], [38].

Thus, using (1), (2) and (3), we can express the SINR of the $N1_n$ - U_{N1}^k , $N2_m$ - U_{N2}^j and BS_i - U_{BS}^t links as

$$\text{SINR}_{U_{N1}^k} = \frac{P_n G_{nU_{N1}^k}^t G_{nU_{N1}^k}^r L_{nk}^S |h_{nk}|^2}{\sum_{m=1}^{N_{S1}} \alpha_m P_m G_{mU_{N1}^k}^t G_{mU_{N1}^k}^r L_{mk}^S |h_{mk}|^2 + \sum_{i \in \Phi_{BS}} P_i L_{ik}^S |h_{ik}|^2 + k_B B_n T_n} \quad (4)$$

and

$$\text{SINR}_{U_{N2}^j} = \frac{P_m G_{mU_{N2}^j}^t G_{mU_{N2}^j}^r L_{mj}^S |h_{mj}|^2}{\sum_{n=1}^{N_{S2}} \alpha_n P_n G_{nU_{N2}^j}^t G_{nU_{N2}^j}^r L_{nj}^S |h_{nj}|^2 + \sum_{i \in \Phi_{BS}} P_i L_{ij}^S |h_{ij}|^2 + k_B B_m T_n} \quad (5)$$

and

$$\text{SINR}_{\text{U}_{\text{BS}}^i} = \frac{P_i L_{it}^S |h_{it}|^2}{\sum_{n=1}^{N_{\text{S3}}} \alpha_n P_n L_{nt}^S |h_{nt}|^2 + \sum_{m=1}^{N_{\text{S4}}} \alpha_m P_m L_{mt}^S |h_{mt}|^2 + \sum_{z \in \Phi_{\text{BS}}, z \neq i} P_z L_{zt}^S |h_{zt}|^2 + \sigma_n^2}. \quad (6)$$

Generally, although the spectrum sharing between NGSO 1 and NGSO 2 is capable of improving the spectrum efficiency, the coverage overlap between NGSO 1 and NGSO 2 may impose severe interference. As shown in Fig. 2, this interference is analyzed for a pair of NGSO constellations, wherein C/N and $C/(I+N)$ denote the carrier to noise ratio, and carrier-to-interference plus noise ratio, respectively. Observe from Fig. 2 that NGSO 2 may impose excessive interference on NGSO 1, which fluctuates as these satellites move.

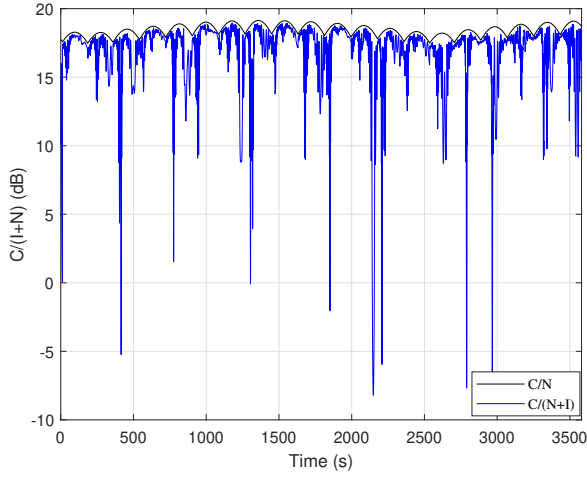


Fig. 2. Co-frequency interference at a typical NGSO 1 imposed by a spectrum-sharing NGSO 2, where the number of satellites in NGSO 1 and NGSO 2 are 648 and 1584, respectively.

As shown in Fig. 3, the intra-constellation CFI of both NGSO 1 and NGSO 2 exist, when the four-color frequency-reuse (FR4) multibeam scheme [27] is adopted. By contrast, the intra-constellation CFI of both NGSO 1 and NGSO 2 becomes negligible in the presence of the seven-color frequency-reuse (FR7) multibeam scheme [28] as shown in Fig. 3. This beneficial result is achieved, since the reuse protection distance of the same frequency is high enough. We should point out that the inter-constellation CFI is neglected in Fig. 3, and we only take the intra-constellation CFI into account. By contrast, the inter-constellation CFI may be more severe than the intra-constellation CFI. Thus, we focus our attention on the inter-constellation CFI in this paper.

B. Coverage Analysis

In this subsection, we analyze the satellite coverage. Given the l -th beam of the satellite $N1_n$, denoted by $b_{N1_n}^l$, its coverage is shown in Fig. 4.

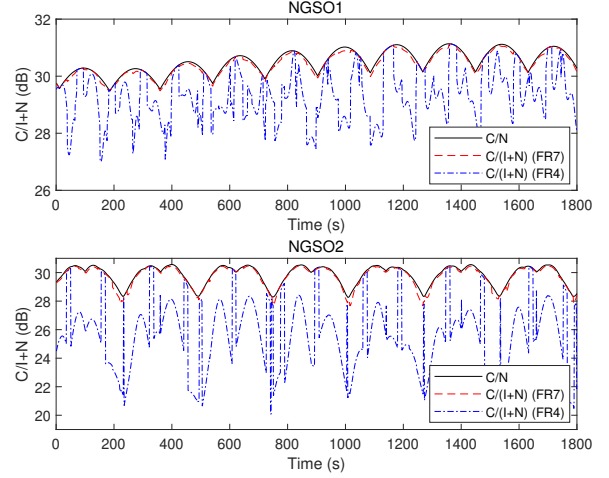


Fig. 3. Intra-constellation co-frequency interference at a typical NGSO 1 and NGSO 2, wherein the FR4 multibeam and the FR7 multibeam are respectively analyzed, the number of satellites in NGSO 1 and NGSO 2 are respectively 648 and 1584, and the inter-constellation co-frequency interference is neglected.

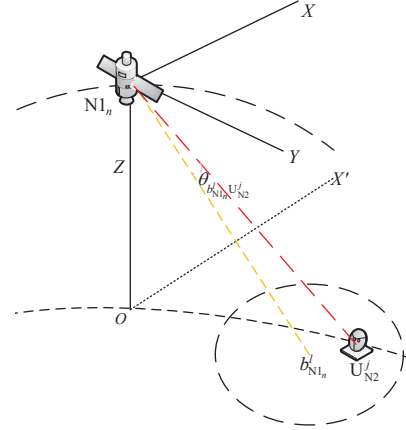


Fig. 4. The coverage analysis for an NGSO 1 satellite.

Given $N1_n$ and U_{N2}^j , the condition of $N1_n$ covering U_{N2}^j can be summarized as

$$\begin{aligned} C_{N1_n U_{N2}^j} = & \left\{ \left(l_{U_{N2}^j}^a, l_{U_{N2}^j}^o, l_{N1_n}^o \right) : \right. \\ & \theta^E \left(l_{U_{N2}^j}^a, l_{U_{N2}^j}^o, l_{N1_n}^o \right) > 0^\circ \\ & \& \theta^A \left(l_{U_{N2}^j}^a, l_{U_{N2}^j}^o, l_{N1_n}^o \right) \in [-180^\circ, 180^\circ] \\ & \left. \& d_{N1_n U_{N2}^j} \leq d_{N1_n}^{\max} \& \theta_{b_{N1_n}^l U_{N2}^j} \leq \frac{\theta^{\text{BW}}}{2} \right\}, \quad (7) \end{aligned}$$

where $\theta^E(l_{U_{N2}^j}^a, l_{U_{N2}^j}^o, l_{N1_n}^o)$ and $\theta^A(l_{U_{N2}^j}^a, l_{U_{N2}^j}^o, l_{N1_n}^o)$ denote the elevation angle and the azimuth angle from U_{N2}^j to $N1_n$, respectively. Furthermore, $d_{N1_n U_{N2}^j}$ is the distance between $N1_n$ and U_{N2}^j , while $d_{N1_n}^{\max}$ represents the distance between $N1_n$ and the border of its beam $b_{N1_n}^l$. Still referring to the above equation, θ^{BW} is the covering angle of a beam of the $N1_n$, and $\theta_{b_{N1_n}^l U_{N2}^j}$ denotes the angle between the link $N1_n \rightarrow$ the center of $b_{N1_n}^l$ and the link $N1_n \rightarrow$ the U_{N2}^j .

Similarly, given $N1_n, N2_m, U_{N1}^k$, and U_{BS}^t , the conditions of $N2_m$ covering U_{N1}^k , of $N1_n$ covering U_{BS}^t , of $N2_m$ covering U_{BS}^t can be summarized.

To elaborate further, given U_{N1}^k, U_{N2}^j and U_{BS}^t , using the above coverage conditions, the NGSO 2 satellite set $\Phi_{N2_m \rightarrow U_{N1}^k}$ covering U_{N1}^k , the NGSO 2 satellite set $\Phi_{N2_m \rightarrow U_{N2}^j}$ covering U_{N2}^j , the NGSO 2 satellite set $\Phi_{N2_m \rightarrow U_{BS}^t}$ covering U_{BS}^t , the NGSO 1 satellite set $\Phi_{N1_n \rightarrow U_{N1}^k}$ covering U_{N1}^k , the NGSO 1 satellite set $\Phi_{N1_n \rightarrow U_{N2}^j}$ covering U_{N2}^j and the NGSO 1 satellite set $\Phi_{N1_n \rightarrow U_{BS}^t}$ covering U_{BS}^t can finally be obtained. By exploiting the number of satellites in the sets $\Phi_{N2_m \rightarrow U_{N1}^k}, \Phi_{N1_n \rightarrow U_{N2}^j}, \Phi_{N1_n \rightarrow U_{BS}^t}$ and $\Phi_{N2_m \rightarrow U_{BS}^t}, N_{S1}, N_{S2}, N_{S3}$ and N_{S4} can also be found.

C. Co-Frequency Exclusion Zone

Based on the above coverage analysis, we exploit the CFEZ for CFI management, especially for managing the co-line interference. Specifically, a pair of spectrum-sharing satellites in a CFEZ may impose excessive interference on each others' users, which may result in call-dropping. As shown in Fig. 5, we consider the NGSO 1 satellite $N1_n$, the NGSO 2 satellite $N2_m$, and their users U_{N1}^k and U_{N2}^j . Moreover, an angle $\theta_{N1_n U_{N1}^k N2_m}$, between $N1_n \rightarrow U_{N1}^k$ and $N2_m \rightarrow U_{N1}^k$, is used to detect the event that $N2_m$ enters into the CFEZ of $N1_n$. Such an angle $\theta_{N1_n U_{N1}^k N2_m}$ is formulated as

$$\theta_{N1_n U_{N1}^k N2_m} = \arccos \left(\frac{d_{N1_n U_{N1}^k}^2 + d_{N2_m U_{N1}^k}^2 - d_{N1_n N2_m}^2}{2d_{N1_n U_{N1}^k} d_{N2_m U_{N1}^k}} \right), \quad (8)$$

where $d_{N1_n N2_m}$ can be expressed by

$$d_{N1_n N2_m} = \sqrt{(X_{N1_n} - X_{N2_m})^2 + (Y_{N1_n} - Y_{N2_m})^2 + (Z_{N1_n} - Z_{N2_m})^2}, \quad (9)$$

where $\{X_{N1_n}, Y_{N1_n}, Z_{N1_n}\}$ and $\{X_{N2_m}, Y_{N2_m}, Z_{N2_m}\}$ respectively denote the locations of $N1_n$ and $N2_m$, which can be specified in the earth-centered earth-fixed coordinate system. Given the calculated $\theta_{N1_n U_{N1}^k N2_m}$, if we have $\theta_{N1_n U_{N1}^k N2_m} < \theta_{CFEZ}$, then spectrum sharing between these two satellites is disabled, and this zone is defined as the CFEZ.

D. Problem Formulation

In order to support spectrum sharing for the SGIN considered while managing the corresponding CFI, the optimization problem is formulated as

$$\begin{aligned} & \max_{P_n, P_m, P_i, N_{S1}, N_{S2}, N_{S3}, N_{S4}} \text{SINR}_{U_{N1}^k} \\ \text{s.t.} \quad & 0 \leq P_n \leq P_{\text{NGSO1}}^{\max} \\ & 0 \leq P_m \leq P_{\text{NGSO2}}^{\max} \\ & 0 \leq P_i \leq P_{\text{BS}}^{\max} \\ & \text{SINR}_{U_{N2}^j} \geq \phi_{th} \\ & \text{SINR}_{U_{BS}^t} \geq \phi_{th} \\ & \alpha_n, \alpha_m \in \{0, 1\}, \end{aligned} \quad (10)$$

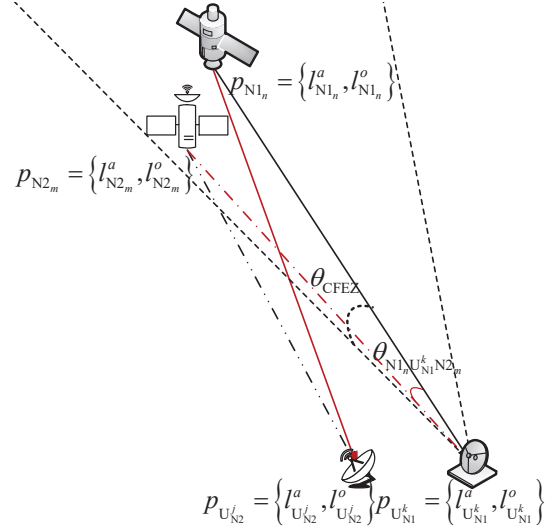


Fig. 5. Co-frequency exclusion zone analysis.

where $P_{\text{NGSO1}}^{\max}, P_{\text{NGSO2}}^{\max}$, and P_{BS}^{\max} are the maximum available transmit power of NGSO 1, of NGSO 2, and of the BSs, respectively, while ϕ_{th} is the minimum SINR required.

Note that optimizing the the k -th user's performance is expected to affect the interference imposed on its neighbors in NGSO 1. However, as mentioned, the effect of the intra-constellation CFI may be negligible in the presence of the multi-color multibeam frequency-reuse schemes (e.g., FR7) as shown in Fig. 3. More explicitly, optimizing the SINR of a user k does not substantially increase the interference imposed on users at the same frequency of a user k in NGSO 1. Similarly, the SINR of a user k may not be obviously affected when optimizing the SINR of other users accessing the same frequency of this user k . Thus, although there may exist a number of users in NGSO 1, the SINR of other users can be optimized similarly to the k -th user, $1 \leq k \leq K$.

This optimization problem is related with the coverage of a pair of NGSO constellations. In the overlapping coverage, given the tele-traffic states, the CSI, and the transmission requirements, the achievable SINR depends both on the beam-scheduling and power-scheduling. It is challenging to directly solve such a complex problem, which hinges on both the coverage analysis and beam-power scheduling.

III. JOINTLY UTILIZING MULTI-DOMAIN RESOURCES FOR INTERFERENCE MANAGEMENT

In this section, we present our multi-domain resource aided interference management scheme, including both beam shut-off and beam switching based scheduling, as well as our LSTM-ARMA-DQN based power allocation.

A. Shut-Off and Switching-Based Beam Scheduling

In this subsection, we conceive a shut-off and switching-based beam scheduling method for managing the CFI. Specifically, using the Poisson traffic-generation model of [25] for NGSO 1 and NGSO 2, the tele-traffic states of the satellites in $\Phi_{N2_m \rightarrow U_{N1}^k}$, and $\Phi_{N2_m \rightarrow U_{N2}^j}$, can be readily estimated. Given

on the estimated tele-traffic states, the idle beams of $N1_n$ and of $N2_m$ are shut off for reducing the amount of interference imposed on NGSO 1's users. As for the active beams of the satellites in $\Phi_{N2_m \rightarrow U_{N1}^k}$, we perform beam switching. More specifically, if there is a satellite $N2_{m'}, m' \neq m$ in $\Phi_{N2_m \rightarrow U_{N2}^j}$ having an idle co-frequency beam, which is not covering U_{N1}^k ($N2_{m'} \notin \Phi_{N2_m \rightarrow U_{N1}^k}$), the $N2_m$ forwards its traffic to this $N2_{m'}$ and informs U_{N2}^j . Then, $N2_{m'}$ may point its beam to U_{N2}^j , and sends the data received from $N2_m$ to U_{N2}^j . As expected, the beam switching action of NGSO 1 is similar to that of NGSO 2. Additionally, the specific procedure of the shut-off and switching based beam scheduling designed is summarized in Algorithm 1.

Algorithm 1: Beam Shut-Off and Beam Switching

Input: $\Phi_{N2_m \rightarrow U_{N1}^k}, \Phi_{N2_m \rightarrow U_{N2}^j}, \Phi_{N1_n \rightarrow U_{N2}^j}, \Phi_{N1_n \rightarrow U_{BS}^t}$ and $\Phi_{N2_m \rightarrow U_{BS}^t}, p(N2_m), p(N1_n), p(U_{N1}^k), p(U_{N2}^j), p(BS_i), p(U_{BS}^t)$ and the traffic states of the $N1_n$ and $N2_m$.

1. Turn off the co-frequency beams of the satellites in $\Phi_{N2_m \rightarrow U_{N1}^k}$ and $\Phi_{N1_n \rightarrow U_{N2}^j}$, if these beams have no active traffic in a given time slot.

2. Remove the satellites from $\Phi_{N2_m \rightarrow U_{N1}^k}$ and $\Phi_{N1_n \rightarrow U_{N2}^j}$, if their beams are turned off in Step 1.

3. If idle beams of the satellites in $\Phi_{N2_m \rightarrow U_{N2}^j}$ are available, and there is one idle beam without covering U_{N1}^k , then

4. Switch the interfering beams of the satellites in $\Phi_{N2_m \rightarrow U_{N1}^k}$ having traffic to idle beams of the satellites in $\Phi_{N2_m \rightarrow U_{N2}^j}$.

5. Remove the satellites from $\Phi_{N2_m \rightarrow U_{N1}^k}$, if their beams are switched in Step 4.

6. End

7. If idle beams of the satellites in $\Phi_{N1_n \rightarrow U_{N1}^k}$ are available, and there is one idle beam without covering U_{N2}^j , then

8. Switch the interfering beams of the satellites in $\Phi_{N1_{n'} \rightarrow U_{N2}^j}, n' \neq n$, having active traffic to idle beams of satellites, similarly to Step 4.

9. End

10. Obtain the updated $\Phi_{N2_m \rightarrow U_{N1}^k}$ and $\Phi_{N1_n \rightarrow U_{N2}^j}$.

11. Obtain the updated $\Phi_{N1_n \rightarrow U_{BS}^t}$ and $\Phi_{N2_m \rightarrow U_{BS}^t}$.

12. Repeat Step 1~7 for different $N1_n$, and its users.

Output: The number of interfering satellites $N'_{S1}, N'_{S2}, N'_{S3}$ and N'_{S4} .

Furthermore, the optimization problem (10), can be simplified as

$$\begin{aligned}
 & \max_{P_n, P_m, P_i} \text{SINR}'_{U_{N1}^k} \\
 \text{s.t.} \quad & 0 \leq P_n \leq P_{\text{NGSO1}}^{\max} \\
 & 0 \leq P_m \leq P_{\text{NGSO2}}^{\max} \\
 & 0 \leq P_i \leq P_{\text{BS}}^{\max} \\
 & \text{SINR}'_{U_{N2}^j} \geq \phi_{\text{th}} \\
 & \text{SINR}'_{U_{BS}^t} \geq \phi_{\text{th}}, \quad (11)
 \end{aligned}$$

where $\text{SINR}'_{U_{N1}^k}, \text{SINR}'_{U_{N2}^j}$ and $\text{SINR}'_{U_{BS}^t}$ are

$$\frac{P_n G_{mU_{N1}^k}^t G_{mU_{N1}^k}^r L_{m,k}^S |h_{m,k}|^2}{\sum_{m=1}^{N'_{S1}} P_m G_{mU_{N1}^k}^t G_{mU_{N1}^k}^r L_{m,k}^S |h_{m,k}|^2 + \sum_{i \in \Phi_{BS}} P_i L_{i,k}^S |h_{i,k}|^2 + k_B B_n T_n}$$

$$\frac{P_m G_{mU_{N2}^j}^t G_{mU_{N2}^j}^r L_{m,j}^S |h_{m,j}|^2}{\sum_{n=1}^{N'_{S2}} P_n G_{nU_{N2}^j}^t G_{nU_{N2}^j}^r L_{n,j}^S |h_{n,j}|^2 + \sum_{i \in \Phi_{BS}} P_i L_{i,j}^S |h_{i,j}|^2 + k_B B_m T_m}$$

and

$$\frac{P_i L_{i,t}^S |h_{i,t}|^2}{\sum_{n=1}^{N'_{S3}} P_n L_{n,t}^S |h_{n,t}|^2 + \sum_{m=1}^{N'_{S4}} P_m L_{m,t}^S |h_{m,t}|^2 + \sum_{z \in \Phi_{BS}, z \neq i} P_z L_{z,t}^S |h_{z,t}|^2 + \sigma_n^2}$$

respectively.

B. LSTM-ARMA-DQN Based Power Allocation

As shown in Fig. 6, a LSTM-ARMA-DQN neural network, combining a LSTM-ARMA and a DQN, is designed for assisting power allocation. Such a LSTM-ARMA model is constructed for predicting the instantaneous CSIs of the links spanning from the satellites to the terrestrial users, using the historical CSIs estimated with the aid of [31]. Explicitly, the LSTM is used, since it does well in time series prediction [41]. To further improve the prediction performance of the LSTM, the ARMA is used for optimizing the prediction error [11], [34], and for upgrading the loss of the LSTM in the model-training stage, since the ARMA is proficient at evaluating the prediction error [42] relying on the parameters of the autoregressive model and the moving average model [32]. Using the upgraded loss and the back propagation algorithm [43], the LSTM can be further optimized. Moreover, the predicted CSIs may be entered into the DQN constructed [33]. Following our previous work [11], [34], the model constructed is optimized with the aid of grid search and K-fold cross-validation. Specifically, the CSI dataset is first divided into K subsets. Then, given the k -th K-fold Cross-Validation, the k -th subset and the remaining subsets are used for validating and training the constructed model, respectively. Additionally, the parameters of the LSTM-ARMA-DQN are optimized with the aid of the adaptive moment estimation optimizer of [34]. The optimized LSTM is composed by two LSTM layers. Their size is 128 and 64. Meanwhile, the optimized DQN is composed by six fully connected (FC) layers, wherein the Rectified Linear Unit function is used as the activation function for each layer of the first three FC layers, and the Hyperbolic Tangent function is utilized as the activation function for each layer of the last three FC layers. The size of six FC layers are 256, 256, 512, 512, 1024 and 1024. Then, the LSTM-ARMA-DQN model is used for optimizing the P_n, P_m and P_i . The specific optimization procedure is summarized in Algorithm 2.

We should point out that our deep-learning-based power allocation algorithm can be used to perform power allocation for the SGIN considered, without requiring channel estimation. In our algorithm, the deep-learning model conceived can predict the CSI, and allocates the transmit power to the SGIN considered. More specifically, due to the propagation delay and the potential co-frequency interference among users, the estimated CSI may become outdated and imperfect. As a remedy, this deep-learning-based power allocation algorithm may be adopted. With the improvement of the computing capability and the multi-access edge computing technology on board satellites [35], [36], this algorithm may be performed on satellites, to avoid the propagation delay between the satellites and the gateways, if the algorithm is executed in the gateways.

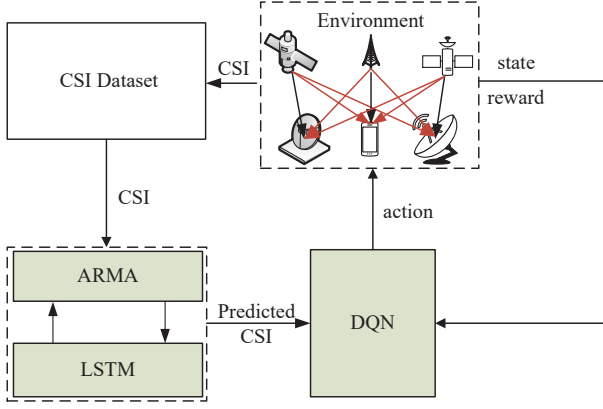


Fig. 6. LSTM-ARMA-DQN aided power allocation.

Algorithm 2: LSTM-ARMA-DQN Based Power Allocation

Input: $\Phi_{N2m} \rightarrow U_{N1}^k$, $\Phi_{N2m} \rightarrow U_{N2}^j$, $\Phi_{N1n} \rightarrow U_{N1}^k$, $\Phi_{N1n} \rightarrow U_{N2}^j$, $\Phi_{N2m} \rightarrow U_{BS}^t$, $\Phi_{N1n} \rightarrow U_{BS}^t$, $p(N2m)$, $p(N1n)$, $p(BS_i)$, $p(U_{N1}^k)$, $p(U_{N2}^j)$, $p(U_{BS}^t)$, P_{NGSO1}^{\max} , P_{NGSO2}^{\max} , P_{BS}^{\max} , and ϕ_{th} .

1. Initialize the parameters of the LSTM-ARMA-DQN model constructed, the transmit power vector \mathbf{P}_n , the SINR vector \mathbf{S}_{SINR} , the SINR threshold $SINR_{UN1}^{max}$, the greedy probability threshold ϵ -greedy.
2. Construct the LSTM-ARMA-DQN model, and train the LSTM-ARMA model constructed.
3. Calculate the antenna gain G_{ab}^d , using the input satellite sets and the locations.
4. Predict the CSIs using the well-trained LSTM-ARMA model at a given transmission slot.
5. Calculate the $SINR_{U_{BS}^t}$, and compare it with ϕ_{th} to adjust P_i , and calculate the required P_m according to the transmission specifications.
6. Calculate the $SINR_{U_{N1}^k}$ using the initialized P_n , the obtained P_i and P_m , and assign the calculated $SINR_{U_{N1}^k}$ to \mathbf{S}_{SINR} .
7. Set a positive reward if the calculated $SINR_{U_{N1}^k} \geq SINR_{UN1}^{max}$ and $P_m \leq P_{NGSO2}^{\max}$, otherwise give a negative reward.
8. Select the max value of the DQN output, assign the index of the selected value to INDEX, if $RAND(0,1) > \epsilon$ -greedy. Otherwise, set INDEX to a random integer value.
9. Update P_n by selecting a value from \mathbf{P}_n using INDEX.
10. Repeat Step 5 ~ 9, until the maximum number of iterations is reached.
11. Obtain the optimized P_n , P_m and P_i using \mathbf{S}_{SINR} , and repeat Step 3 ~ 10 for different $N1_n$.

Output: The optimized P_n^o , P_m^o , and P_i^o .

IV. OUTAGE PROBABILITY ANALYSIS FOR THE PROPOSED JMDR-IM SCHEME

In this section, we derive the OP of the proposed JMDR-IM scheme. Moreover, we also provide the asymptotic OP analysis of the proposed JMDR-IM scheme.

Using [39], the definition of the OP is given by

$$P_{OP} = \Pr(SINR < \phi_{th}). \quad (12)$$

A. NGSO 1 Outage Probability Analysis

Using (4) and (12), the OP of the $N1_n-U_{N1}^k$ link in the proposed JMDR-IM scheme is written as

$$P_{OP}^{NGSO1} = \Pr \left(\frac{P_n^o G_{nU_{N1}^k}^t G_{nU_{N1}^k}^r L_{nk}^S |h_{nk}|^2}{\sum_{m=1}^{N_{S1}'} P_m^o G_{mU_{N1}^k}^t G_{mU_{N1}^k}^r L_{mk}^S |h_{mk}|^2 + \sum_{i \in \Phi_{BS}} P_i^o L_{ik}^S |h_{ik}|^2 + \sigma_{N1}^2} < \phi_{th} \right), \quad (13)$$

where we have $\sigma_{N1}^2 = k_B B_n T_n$, $L_{iU_{N1}^k}^S = L_{iU_{N1}^k}^{-\alpha_t}$, α_t is the path loss exponent, and $L_{iU_{N1}^k}$ is the distance between the BS_i and the U_{N1}^k .

Using (A.7), P_{OP}^{NGSO1} can be finally obtained.

To further explore the OP of the $N1_n-U_{N1}^k$ link in the proposed JMDR-IM scheme, we analyze the asymptotic outage probability (AOP). The PDF of $P_n |h_{nk}|^2$ can be formulated as

$$f_{P_n |h_{nk}|^2}(x) = \frac{\alpha_{N1n}}{P_n} e^{-\beta_{N1n} \frac{x}{P_n}} {}_1F_1 \left(m_{N1n}; 1; \delta_{N1n} \frac{x}{P_n} \right). \quad (14)$$

For a large P_n , we have ${}_1F_1(m_{N1n}; 1; \delta_{N1n} \frac{x}{P_n}) \rightarrow 1$ [39]. Thus, $f_{P_n |h_{nk}|^2}(x)$ can be rewritten as

$$f_{P_n |h_{nk}|^2}(x) = \frac{\alpha_{N1n}}{P_n} e^{-\beta_{N1n} \frac{x}{P_n}}. \quad (15)$$

Using (15), similarly to (A.7), the AOP of the $N1_n-U_{N1}^k$ link in the proposed JMDR-IM scheme can be expressed as

$$P_{AOP}^{NGSO1} = \frac{\alpha_{N1n}}{\beta_{N1n}} \prod_{m=1}^{N_{S1}'} \sum_{n_{N2m}=0}^{m_{N2m}-1} Z_{N2m} - \frac{\alpha_{N1n}}{\beta_{N1n}} e^{-\frac{\beta_{N1n}}{P_n} S' \sigma_{N1}^2} \prod_{m=1}^{N_{S1}'} \sum_{n_{N2m}=0}^{m_{N2m}-1} \frac{Z_{N2m} (\beta_{N2m} - \delta_{N2m})}{(\beta_{N1n} - \delta_{N1n} + \frac{\beta_{N1n}}{P_n} \zeta'_m)^{n_{N2m}+1}} \prod_{i=1}^{N_{BS}} \frac{1}{\sigma_{BS}^2 \left(\frac{\beta_{N1n}}{P_n} I'_{BS} + \frac{1}{\sigma_{BS}^2} \right)}, \quad (16)$$

$$\text{where } \zeta'_m = \frac{\phi_{th} G_{mU_{N1}^k}^t G_{mU_{N1}^k}^r L_{mk}^S P_m}{G_{nU_{N1}^k}^t G_{nU_{N1}^k}^r L_{nk}^S}, \quad S' = \frac{\phi_{th}}{G_{nU_{N1}^k}^t G_{nU_{N1}^k}^r L_{nk}^S} \text{ and } I'_{BS} = \frac{\phi_{th} P_i L_{ik}^S}{G_{nU_{N1}^k}^t G_{nU_{N1}^k}^r L_{nk}^S}.$$

We should point out that the OP of NGSO 1 can be dramatically reduced. This beneficial result is achieved because the SINR of NGSO 1 can be increased by the JMDR-IM scheme, and an increased SINR results in an OP reduction.

B. NGSO 2 Outage Probability Analysis

Moreover, using (5) and (12), the OP of the N_{2m} - $U_{N_2}^j$ link in the proposed JMDR-IM scheme is formulated as

$$P_{OP}^{NGSO2} = \Pr \left(\frac{P_m^o G_{mU_{N_2}^j}^t G_{mU_{N_2}^j}^r L_{mj}^S |h_{mj}|^2}{\sum_{n=1}^{N_{S2}'} P_n^o G_{nU_{N_2}^j}^t G_{nU_{N_2}^j}^r L_{nj}^S |h_{nj}|^2 + \sum_{i \in \Phi_{BS}} P_i L_{ij}^S |h_{ij}|^2 + \sigma_{N_2}^2} < \phi_{th} \right), \quad (17)$$

where $\sigma_{N_2}^2 = k_B B_m T_n$, $L_{ij}^S = L_{iU_{N_2}^j}^{-\alpha_t}$ and $L_{iU_{N_2}^j}$ is the distance between BS_i and $U_{N_2}^j$.

Similarly to (A.7), P_{OP}^{NGSO2} can be formulated as

$$\begin{aligned} P_{OP}^{NGSO2} &= \sum_{n_{N_2m}=0}^{m_{N_2m}-1} \left(Z_{N_2m} \prod_{n=1}^{N_{S2}'} \sum_{n_{N_1n}=0}^{m_{N_1n}-1} Z_{N_1n} - Z_{N_2m} e^{-(\beta_{N_2m} - \delta_{N_2m})} S \sigma_{N_2}^2 \right. \\ &\quad \sum_{k_o=0}^{n_{N_1n}} \sum_{j_o=0}^{k_o} \sum_{z_o=0}^{j_o} \frac{(\beta_{N_2m} - \delta_{N_2m})^{k_o}}{k_o!} \binom{k_o}{j_o} \binom{j_o}{z_o} (S_1 \sigma_{N_2}^2)^{j_o - z_o} \\ &\quad \sum_{x_n \geq 0, x_1, x_2, \dots, x_{N_{S2}'}} \binom{k_o - j_o}{x_1, x_2, \dots, x_{N_{S2}'}} \prod_{n=1}^{N_{S2}'} (\zeta_n)^{x_n} \\ &\quad \prod_{n=1}^{N_{S2}'} \left(\sum_{n_{N_1n}=0}^{m_{N_1n}-1} Z_{N_1n} (\beta_{N_1n} - \delta_{N_1n}) (x_n + n_{N_1n})! \right. \\ &\quad \left. \left((\beta_{N_2m} - \delta_{N_2m}) \zeta_n - (\beta_{N_1n} - \delta_{N_1n}) \right)^{-x_n - n_{N_1n} - 1} \right. \\ &\quad \left. \sum_{y_i \geq 0, y_1, y_2, \dots, y_{N_{BS}}} z_y \prod_{i=1}^{N_{BS}} (I_{BS_i})^{y_i} \prod_{i=1}^{N_{BS}} \frac{1}{\sigma_{BS}^2} (y_i)! \right. \\ &\quad \left. \left((\beta_{N_2m} - \delta_{N_2m}) I_{BS_1} + \frac{1}{\sigma_{BS}^2} \right)^{-y_i - 1} \right) \Bigg), \quad (18) \end{aligned}$$

where we have $Z_{N_2m} = \frac{\alpha_{N_2m} (m_{N_2m} - 1)! (\delta_{N_2m})^{n_{N_2m}}}{(m_{N_2m} - 1 - n_{N_2m})! (1)_{n_{N_2m}} (\beta_{N_2m} - \delta_{N_2m})^{n_{N_2m} + 1}}$, $\zeta_n = \frac{\phi_{th} P_n^o G_{nU_{N_2}^j}^t G_{nU_{N_2}^j}^r L_{nj}^S}{P_m^o G_{mU_{N_2}^j}^t G_{mU_{N_2}^j}^r L_{mj}^S}$, $I_{BS_1} = \frac{\phi_{th} P_i^o L_{ij}^S}{P_m^o G_{mU_{N_2}^j}^t G_{mU_{N_2}^j}^r L_{mj}^S}$, and $S_1 = \frac{\phi_{th}}{P_m^o G_{mU_{N_2}^j}^t G_{mU_{N_2}^j}^r L_{mj}^S}$.

To evaluate the OP of a large P_m , similarly to (16), the AOP of the N_{2m} - $U_{N_2}^j$ link in the proposed JMDR-IM scheme

can be expressed as

$$\begin{aligned} P_{AOP}^{NGSO2} &= \frac{\alpha_{N_2m}}{\beta_{N_2m}} \prod_{n=1}^{N_{S2}'} \sum_{n_{N_1n}=0}^{m_{N_1n}-1} Z_{N_1n} - \frac{\alpha_{N_2m}}{\beta_{N_2m}} e^{-\frac{\beta_{N_2m}}{P_m} S_1' \sigma_{N_2}^2} \\ &\quad \prod_{n=1}^{N_{S2}'} \sum_{n_{N_1n}=0}^{m_{N_1n}-1} Z_{N_1n} (\beta_{N_1n} - \delta_{N_1n}) \\ &\quad \left(\beta_{N_2m} - \delta_{N_2m} + \frac{\beta_{N_2m}}{P_m} \zeta_n' \right)^{-n_{N_1n} - 1} \\ &\quad \prod_{i=1}^{N_{BS}} \frac{1}{\sigma_{BS}^2 \left(\frac{\beta_{N_2m}}{P_m} I_{BS_1}' + \frac{1}{\sigma_{BS}^2} \right)}, \quad (19) \end{aligned}$$

where $\zeta_n' = \frac{\phi_{th} G_{nU_{N_2}^j}^t G_{nU_{N_2}^j}^r L_{nj}^S P_n}{G_{mU_{N_2}^j}^t G_{mU_{N_2}^j}^r L_{mj}^S}$, $S_1' = \frac{\phi_{th}}{G_{mU_{N_2}^j}^t G_{mU_{N_2}^j}^r L_{mj}^S}$, and $I_{BS_1}' = \frac{\phi_{th} P_i L_{ik}^S}{G_{mU_{N_2}^j}^t G_{mU_{N_2}^j}^r L_{mj}^S}$.

C. BS Outage Probability Analysis

Meanwhile, using (6) and (12), the OP of the BS_i - U_{BS}^t link in the proposed JMDR-IM scheme is written as

$$P_{OP}^{BS} = \Pr \left(\frac{P_i^o L_{it}^S |h_{it}|^2}{\sum_{n=1}^{N_{S3}'} P_n^o G_{nU_{BS}^t}^t L_{nt}^S |h_{nt}|^2 + \sum_{m=1}^{N_{S4}'} P_m^o L_{mt}^S G_{mU_{BS}^t}^t |h_{mt}|^2 + \sum_{j \in \Phi_{BS}, j \neq i} P_j^o L_{jt}^S |h_{jt}|^2 + \sigma_{N_2}^2} < \phi_{th} \right), \quad (20)$$

where we have $L_{it}^S = L_{iU_{BS}^t}^{-\alpha_t}$, $L_{jt}^S = L_{jU_{BS}^t}^{-\alpha_t}$, with $L_{iU_{BS}^t}$ and $L_{jU_{BS}^t}$ representing the distance between BS_i and U_{BS}^t , as well as between BS_j and U_{BS}^t .

Using (A.1)-(A.3), P_{OP}^{BS} can be obtained as

$$\begin{aligned} P_{OP}^{BS} &= \prod_{n=1}^{N_{S3}'} \sum_{n_{N_1n}=0}^{m_{N_1n}-1} Z_{N_1n} \prod_{m=1}^{N_{S4}'} \sum_{n_{N_2m}=0}^{m_{N_2m}-1} Z_{N_2m} - \\ &\quad \prod_{n=1}^{N_{S3}'} \sum_{n_{N_1n}=0}^{m_{N_1n}-1} Z_{N_1n} (\beta_{N_1n} - \delta_{N_1n}) \left(\beta_{N_1n} - \delta_{N_1n} + \frac{A_n}{\sigma_{BS}^2} \right)^{-n_{N_1n} - 1} \\ &\quad \prod_{m=1}^{N_{S4}'} \sum_{n_{N_2m}=0}^{m_{N_2m}-1} Z_{N_2m} (\beta_{N_2m} - \delta_{N_2m}) \left(\beta_{N_2m} - \delta_{N_2m} + \frac{B_m}{\sigma_{BS}^2} \right)^{-n_{N_2m} - 1} \\ &\quad \prod_{j=1, j \neq i}^{N_{BS}} \left(\frac{1}{\sigma_{BS}^2 C_j + 1} \right) \cdot e^{-\frac{1}{\sigma_{BS}^2} D_i}, \quad (21) \end{aligned}$$

where we have $A_n = \frac{\phi_{th} P_n^o G_{nU_{BS}^t}^t L_{nk}^S}{P_i L_{ik}^S}$, $B_m = \frac{\phi_{th} P_m^o G_{mU_{BS}^t}^t L_{mt}^S}{P_i L_{ik}^S}$, $C_j = \frac{\phi_{th} P_j^o L_{jt}^S}{P_i L_{ik}^S}$ and $D_i = \frac{\phi_{th} \sigma_{N_2}^2}{P_i L_{ik}^S}$.

When P_i becomes very large, using (B.3), the AOP of BS_i - U_{BS}^t link in the proposed JMDR-IM scheme can also be obtained.

V. SIMULATION RESULTS

In this section, we evaluate the proposed JMDR-IM scheme in terms of its SINR characteristics and the OP of the SGIN considered, and compare it to the conventional PPAFB scheme. Moreover, the analytic OPs of NGSO 1, of NGSO 2 and of the BSs are evaluated by plotting (A.7), (18) and (21), respectively. The simulated OPs of NGSO 1, of NGSO 2 and of the BSs are also provided to verify the accuracy of the analytic OPs, which are denoted by (S.). Furthermore, the analytic AOPs of NGSO 1, of NGSO 2 and of the BSs, denoted by (A.), are analyzed by plotting (16), (19) and (B.3). The associated simulation parameters are given in Table III. Moreover, the experimental platform is an Intel(R) Core(TM)i7-9700K CPU 3.60GHz, the GPU is NVIDIA RTX2080Ti, and the amount of memory is 64.00GB. The neural network is constructed on the Tensorflow framework. Note that the default number of NGSO constellations is two in the simulations, and these two constellations are NGSO 1 and NGSO 2. Moreover, the size of the dataset employed for both training and testing the LSTM are ten thousand and one-hundred thousand.

TABLE III
SIMULATION PARAMETERS

Parameter	Symbol	Value
NGSO 1 satellite number	N	648
NGSO 2 satellite number	M	1584
NGSO 3 satellite number		720
NGSO 1 satellite antenna diameter	D_{N1_n}	0.4 m
NGSO 2 satellite antenna diameter	D_{N2_m}	0.4 m
NGSO 3 satellite antenna diameter		0.4 m
NGSO 2 user antenna diameter	$D_{U_{N1_k}}$	0.6 m
NGSO 2 user antenna diameter	$D_{U_{N2_j}}$	0.6 m
NGSO 3 user antenna diameter		0.6 m
Antenna efficiency	ξ	55%
Frequency band	f	17.9 GHz
NGSO 1 transmission bandwidth	B_n	125 MHz
NGSO 2 transmission bandwidth	B_m	125 MHz
NGSO 3 transmission bandwidth		125 MHz
NGSO 1 orbit altitude	h_{N1_n}	500 km
NGSO 2 orbit altitude	h_{N2_m}	550 km
NGSO 3 orbit altitude		570 km
Earth radius	R	6370 km
Equivalent noise temperature	T_n	290 K
NGSO 1 maximum transmit power	P_{NGSO1}^{\max}	5 W
NGSO 2 maximum transmit power	P_{NGSO2}^{\max}	5 W
NGSO 3 maximum transmit power		5 W
BS maximum transmit power	P_{BS}^{\max}	5 W
SINR threshold	ϕ_{th}	10 dB
Greedy probability	ε -greedy	0.8
Scattered components's average power	$c_{N1_n}(c_{N2_m})$	0.126
Nakagami fading parameters	$m_{N1_n}(m_{N2_m})$	10.1
LOS components's average power	$\Omega_{N1_n}(\Omega_{N2_m})$	0.835
Channel-gain mean	σ_{BS}^2	1

Figure 7 portrays $\text{SINR}_{U_{N1}^k}$ versus P_{NGSO1}^{\max} parameterized by different θ^{BW} for the proposed JMDR-IM and PPAFB schemes. Observe from Fig. 7 that the proposed JMDR-IM scheme outperforms the conventional PPAFB scheme in terms of its $\text{SINR}_{U_{N1}^k}$ for both $\theta^{BW} = 15^\circ$ and $\theta^{BW} = 7.5^\circ$. Furthermore, the proposed JMDR-IM scheme of $\theta^{BW} = 15^\circ$ achieves a higher $\text{SINR}_{U_{N1}^k}$ than the PPAFB scheme of $\theta^{BW} = 7.5^\circ$. It is also shown in Fig. 7 that the $\text{SINR}_{U_{N1}^k}$ of the JMDR-IM scheme for $\theta^{BW} = 15^\circ$ and of the PPAFB scheme for both $\theta^{BW} = 15^\circ$ and $\theta^{BW} = 7.5^\circ$ tends to be constant. This near-constant $\text{SINR}_{U_{N1}^k}$ is achieved, since

increasing the transmit power of NGSO 1 may increase the interference imposed on the users of NGSO 2 and of the BSs. To meet the transmission requirements of both NGSO 2 and of the BSs, the NGSO 1 satellites are not allowed to increase their transmit power beyond a certain threshold. By contrast, the JMDR-IM scheme can have a higher transmit power, demonstrating the superiority of the JMDR-IM scheme in terms of managing interference. Observe from Fig. 7 that the SINR in the JMDR-IM and the PPAFB schemes are decreased in the presence of the SINR of the JMDR-IM and the PPAFB schemes is reduced in the presence of the intra-constellation CFI, compared to using no intra-constellation CFI. This SINR reduction may be tolerable, especially when more robust multi-color multibeam frequency-reuse schemes are used, such as the FR7 multibeam [28], the eight-color frequency-reuse [29], and the twelve-color frequency-reuse multibeam regimes [30]. Additionally, as shown in Fig. 7, the SINR of both the JMDR-IM and the PPAFB schemes using the predicted CSI approach, as well as that of the JMDR-IM and the PPAFB schemes was quantified by using the actual CSI, showing the effectiveness of the LSTM-ARMA-DQN conceived in terms of predicating the CSI. We also analyze the case when the intra-constellation interference is considered, but the inter-constellation interference is neglected. One can observe from Fig. 7 that this case achieves the highest SINR, albeit at the cost of requiring more spectral resources. This result demonstrates that the effect on the SINR imposed by the inter-constellation CFI is more severe than that inflicted by the intra-constellation CFI in the SGIN considered.

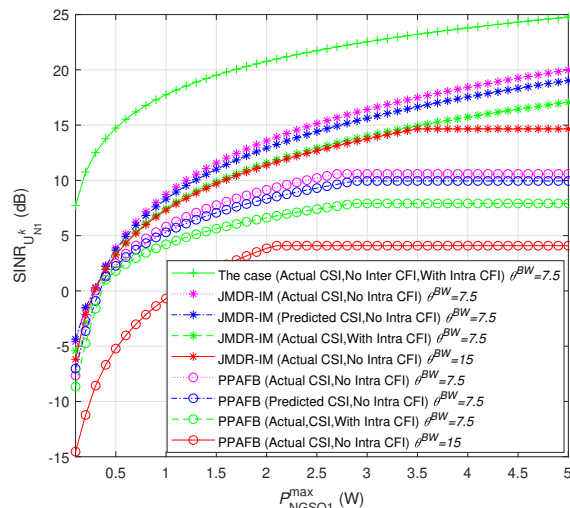


Fig. 7. $\text{SINR}_{U_{N1}^k}$ versus P_{NGSO1}^{\max} parameterized by different θ^{BW} for the proposed JMDR-IM and the conventional PPAFB schemes, wherein the $\text{SINR}_{U_{N1}^k}$ is evaluated by optimizing (11), the effect of the intra-constellation CFI, the actual CSI and the predicted CSI are investigated.

Figure 8 depicts the $\text{SINR}_{U_{N2}^j}^{\min}$ versus P_{NGSO1}^{\max} parameterized by different θ^{BW} for the proposed JMDR-IM and the conventional PPAFB schemes, where $\text{SINR}_{U_{N2}^j}^{\min}$ denotes the lowest SINR of different U_{N2}^j . It is shown from Fig. 8 that the $\text{SINR}_{U_{N2}^j}^{\min}$ of the proposed JMDR-IM scheme is higher than that of the conventional PPAFB scheme, when P_{NGSO1}^{\max}

is lower than 3.5 W. Fig. 8 also shows that although a higher transmit power is available, NGSO 1 relying on the conventional PPAFB scheme may perform wireless transmissions at a limited transmit power for satisfying the transmission requirements of both NGSO 2 and of the BSs. However, the proposed JMDR-IM scheme allows NGSO 1 to perform wireless transmissions at a higher transmit power than the traditional PPAFB scheme, whilst meeting the transmission requirements of both NGSO 2 and of the BSs. This increased transmit power of NGSO 1 can be effectively converted into a SINR improvement of NGSO 1, as shown in Fig. 7.

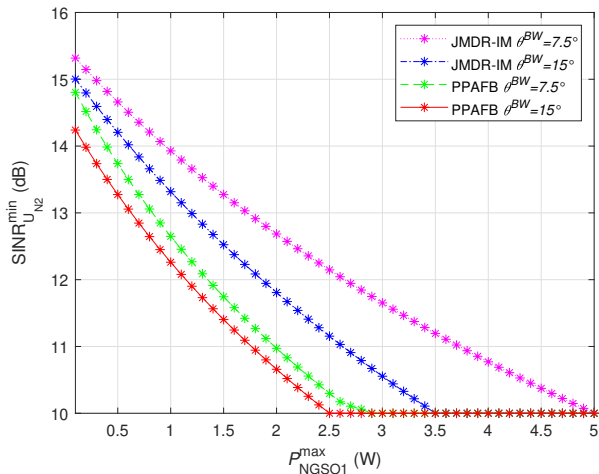


Fig. 8. $\text{SINR}_{U_{N2}}^{\min}$ versus P_{NGSO1}^{\max} parameterized by different θ^{BW} for the proposed JMDR-IM and the conventional PPAFB schemes, wherein NGSO 1 and NGSO 2 constellations are considered.

Figure 9 explores the $\text{SINR}_{U_{N2}}^{\min}$ versus P_{NGSO2}^{\max} parameterized by different number of NGSO constellations for both the proposed JMDR-IM and for the conventional PPAFB schemes. Observe from Fig. 9 that although NGSO 2 relying on both the JMDR-IM and the PPAFB schemes meets the SINR threshold, the required transmit power of NGSO 2 using the JMDR-IM scheme is lower than that of NGSO 2 employing the PPAFB scheme. This is due to the fact that given an SINR threshold, a lower transmit power is required in the presence of lower interference received. These beneficial results indicate that the JMDR-IM scheme effectively manages the interference imposed on the users of NGSO 2. It is also shown from Fig. 9 that as the number of NGSO constellations increases from two to three, the SINR of users in NGSO 2 decreases correspondingly, when using the JMDR-IM and the PPAFB schemes. This result shows that the inter-constellation CFI becomes more severe upon increasing the number of spectrum-sharing NGSO constellations. Fortunately, the proposed JMDR-IM scheme can still meet the transmission requirements even in the presence of three NGSO constellations.

Figure 10 shows the $\text{SINR}_{U_{N1}^k}$ versus P_{NGSO2}^{\max} parameterized by different number of NGSO constellations for both the proposed JMDR-IM, the conventional PPAFB and the pure fixed power based fixed beams (PFPFB) schemes. Similarly to Fig. 9, one can observe from Fig. 10 that although a higher P_{NGSO2}^{\max} is available, the proposed JMDR-IM scheme allocates

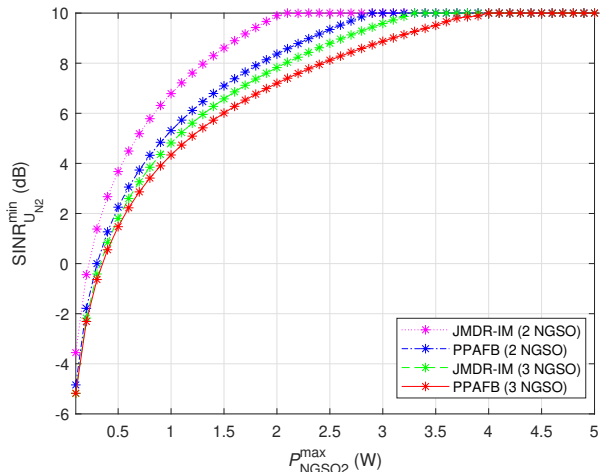


Fig. 9. $\text{SINR}_{U_{N2}}^{\min}$ versus P_{NGSO2}^{\max} parameterized by different number of NGSO constellations for the proposed JMDR-IM and the conventional PPAFB schemes, wherein $\theta^{\text{BW}} = 7.5^\circ$.

a lower transmit power than the PPAFB scheme for NGSO 2. This lower transmit power of NGSO 2 using the JMDR-IM scheme not only readily meets the SINR requirements of NGSO 2, but also reduces the amount of interference imposed on the users of NGSO 1, hence resulting in a higher $\text{SINR}_{U_{N1}^k}$. Fig. 10 also shows that the SINR will be reduced in the presence of three NGSO constellations. However, the proposed JMDR-IM scheme still achieves a higher SINR than the PPAFB and the PFPFB schemes, when the number of spectrum-sharing NGSO constellations is three. Compared to the PPAFB scheme, the performance gain of beam shut-off/beam-switching can be evaluated. This result demonstrates the superiority of the beam shut-off/beam-switching regime in terms of managing the inter-constellation CFI. Moreover, this gain increases upon increasing P_{NGSO2}^{\max} . These beneficial results indicate that the CFI management of beam shut-off/beam-switching and deep-learning-based power allocation harnessed in the proposed JMDR-IM scheme can be effectively converted into SINR enhancements.

In Fig. 11, we investigate $C/(I+N)$ of NGSO 1 at different time instants. Observe from Fig. 2 that NGSO 2 may impose a higher amount of interference on the users of NGSO 1 in the presence of spectrum sharing without using the JMDR-IM scheme. Moreover, the interference imposed by NGSO 2 may fluctuate as the satellites of NGSO 2 move. These interference sources may result in a low and time-varying $C/(I+N)$ for NGSO 1. In contrast to Fig. 2, observe from Fig. 11 that the interference imposed by NGSO 2 is beneficially managed by the proposed JMDR-IM scheme. Additionally, the JMDR-IM scheme can track the time-varying interference, and maintain a high $C/(I+N)$ for NGSO 1. These beneficial results demonstrate the superiority of the proposed JMDR-IM scheme in a spectrum-sharing SGIN in the face of dynamically fluctuating propagation characteristics.

Figure 12 explores $P_{\text{OP}}^{\text{NGSO1}}$ versus the SINR threshold ϕ_{th} parameterized by different θ^{BW} for the proposed JMDR-IM and the conventional PPAFB schemes, wherein $P_{\text{AOP}}^{\text{NGSO1}}$ is

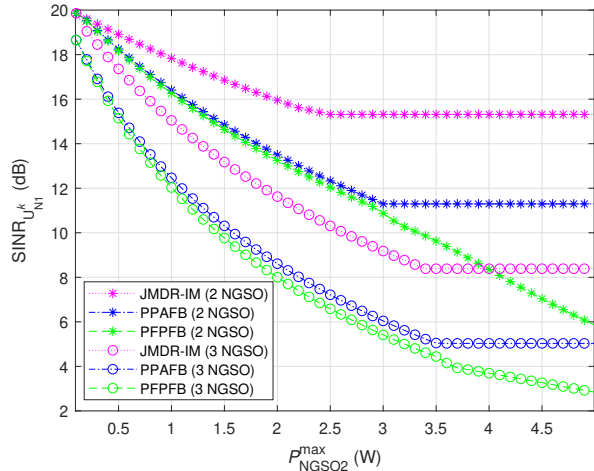


Fig. 10. $\text{SINR}_{U_{N1}}^k$ versus P_{NGSO2}^{\max} parameterized by different number of NGSO constellations for the proposed JMDR-IM, the conventional PPAFB and the PFPFB schemes, wherein $\theta^{\text{BW}} = 7.5^\circ$.

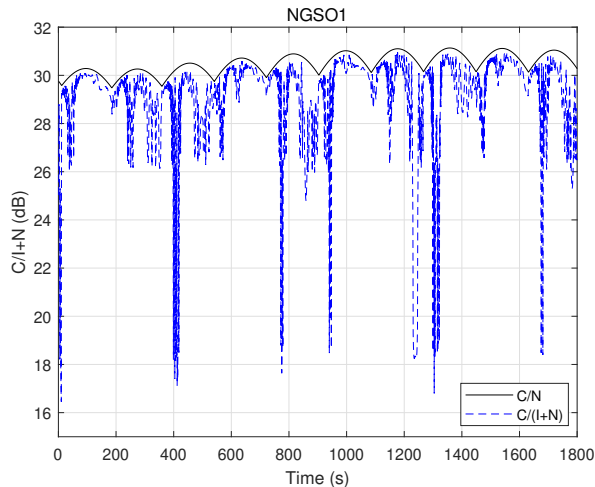


Fig. 11. $C/(I+N)$ of NGSO 1 versus time using the proposed JMDR-IM scheme.

also evaluated. Observe from Fig. 12 that the proposed JMDR-IM scheme outperforms the conventional PPAFB scheme in terms of its OP for both $\theta^{\text{BW}} = 15^\circ$ and $\theta^{\text{BW}} = 7.5^\circ$. Furthermore, given $\phi_{th} = 10$ dB, $P_{\text{AOP}}^{\text{NGSO1}}$ is lower than 10^{-3} . These beneficial results demonstrate the superiority of the JMDR-IM scheme in terms of increasing the reliability of wireless transmissions in the SGIN considered. Fig. 12 also shows that $P_{\text{OP}}^{\text{NGSO1}}$ is close to $P_{\text{AOP}}^{\text{NGSO1}}$ in the low ϕ_{th} region, and $P_{\text{OP}}^{\text{NGSO1}}$ is a bit lower than the $P_{\text{AOP}}^{\text{NGSO1}}$ in the high ϕ_{th} region. Moreover, the analytic $P_{\text{OP}}^{\text{NGSO1}}$ matches the simulated $P_{\text{OP}}^{\text{NGSO1}}$, verifying the accuracy of the analysis.

Figure 13 investigates $P_{\text{OP}}^{\text{NGSO2}}$ versus the SINR threshold ϕ_{th} parameterized by different θ^{BW} for the proposed JMDR-IM and the conventional PPAFB schemes, wherein $P_{\text{AOP}}^{\text{NGSO2}}$ is also evaluated. Observe from Fig. 13 that the proposed JMDR-IM scheme achieves a lower $P_{\text{OP}}^{\text{NGSO2}}$ than the conventional PPAFB scheme. Furthermore, observe from Fig. 13 that given a tolerable OP, the ϕ_{th} of the proposed JMDR-IM scheme is

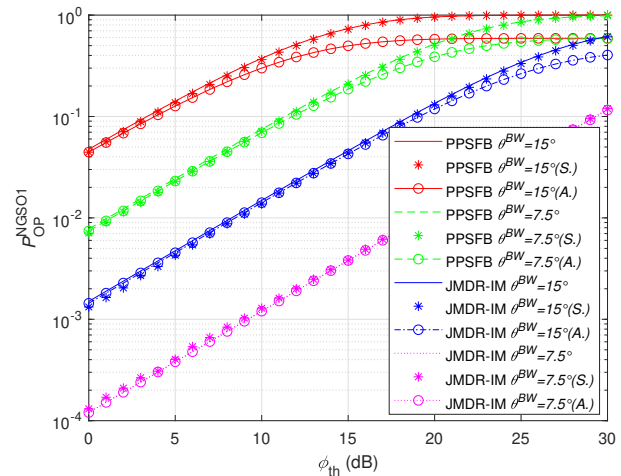


Fig. 12. $P_{\text{OP}}^{\text{NGSO1}}$ versus the SINR threshold ϕ_{th} parameterized by different θ^{BW} for the proposed JMDR-IM and the conventional PPAFB schemes, wherein the analytic $P_{\text{OP}}^{\text{NGSO1}}$ and $P_{\text{AOP}}^{\text{NGSO1}}$ are evaluated by plotting (A.9) and (16), respectively.

higher than that of the conventional PPAFB scheme. This is due to the fact that the proposed JMDR-IM scheme effectively manages the interference received at NGSO 2 and attains a higher SINR than the PPAFB scheme.

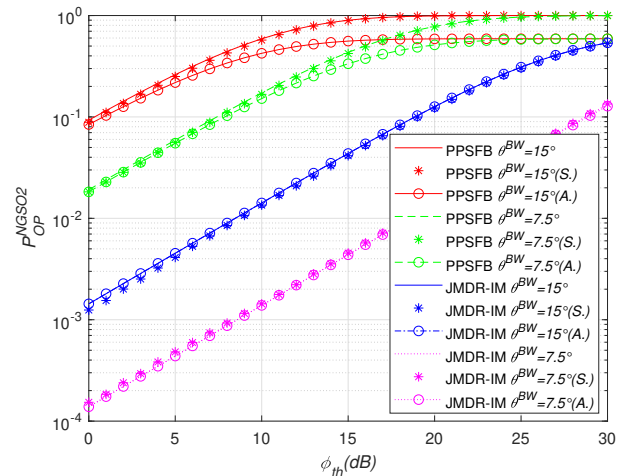


Fig. 13. $P_{\text{OP}}^{\text{NGSO2}}$ versus the SINR threshold ϕ_{th} parameterized by different θ^{BW} for the proposed JMDR-IM and the conventional PPAFB schemes, wherein the analytic $P_{\text{OP}}^{\text{NGSO2}}$ and $P_{\text{AOP}}^{\text{NGSO2}}$ are evaluated by plotting (18) and (19), respectively.

In Fig. 14, we analyze $P_{\text{OP}}^{\text{BS}}$ versus the SINR threshold ϕ_{th} parameterized by different θ^{BW} for the proposed JMDR-IM and the conventional PPAFB schemes, wherein $P_{\text{AOP}}^{\text{BS}}$ is evaluated. As shown in Fig. 14, when the ϕ_{th} is reduced from 30 dB to 0 dB, the $P_{\text{OP}}^{\text{BS}}$ of both the JMDR-IM and PPAFB schemes decreases correspondingly. Moreover, observe from Fig. 14 that for a specific ϕ_{th} , the proposed JMDR-IM scheme still achieves a lower OP for the BSs than the conventional PPAFB scheme, through managing the interference imposed on the users of the BSs. Additionally, the $P_{\text{AOP}}^{\text{BS}}$ equals the $P_{\text{OP}}^{\text{BS}}$ in the low ϕ_{th} region, and the $P_{\text{AOP}}^{\text{BS}}$ becomes lower

than the the P_{OP}^{BS} when the ϕ_{th} is 3 dB. Upon combining Fig. 12~Fig. 14, we can infer that the proposed JMDR-IM scheme simultaneously decreases the OPs of NGSO 1, of NGSO 2 and of the BSs. This significant OP deduction confirms the superiority of the proposed JMDR-IM scheme in terms of managing the interference and increasing the reliability of wireless transmissions.

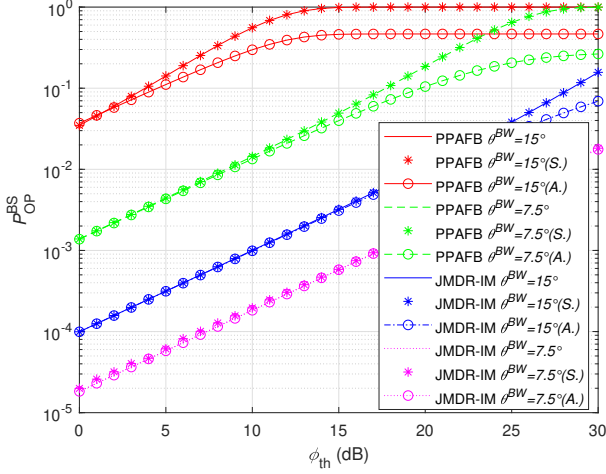


Fig. 14. P_{OP}^{BS} versus the SINR threshold ϕ_{th} parameterized by θ^{BW} for the proposed JMDR-IM and the conventional PPAFB schemes, wherein the analytic P_{OP}^{BS} and P_{AOP}^{BS} are evaluated by plotting (21) and (B.3).

VI. CONCLUSIONS

Spectrum sharing in SGINs is capable of improving the spectrum utilization, which however leads to severe CFI. We proposed the JMDR-IM scheme for managing the CFI, relying on our coverage overlap analysis, and on multi-domain resource scheduling. To be specific, the coverage overlap of a pair of NGSO constellations was analyzed, and the co-frequency exclusion zone concept was harnessed for managing the co-line interference. Then, multi-domain resources were jointly scheduled relying on the analysis results. More specifically, beam shut-off and beam-switching aided scheduling was harnessed for alleviating the CFI. Then, the LSTM-ARMA-DQN scheme was adopted for alleviating the CFI via optimizing the transmit power for NGSO 1, of NGSO 2 and of the BSs. Additionally, the OP was also analyzed, to demonstrate the superiority of the proposed JMDR-IM scheme in terms of guaranteeing reliable transmissions in the SGIN considered.

APPENDIX A DERIVATION OF P_{OP}^{NGSO1}

According to [39], the probability density function (PDF) of the random variables (RVs) $|h_{nk}|^2$, $|h_{mk}|^2$ and $|h_{ik}|^2$ can

be respectively formulated as:

$$\begin{aligned} f_{|h_{nk}|^2}(x) &= \alpha_{N1_n} e^{-\beta_{N1_n} x} {}_1F_1(m_{N1_n}; 1; \delta_{N1_n} x) \\ &= \alpha_{N1_n} e^{-(\beta_{N1_n} - \delta_{N1_n}) x} \\ &\quad \sum_{n_{N1_n}=0}^{m_{N1_n}-1} \frac{(m_{N1_n} - 1)! (\delta_{N1_n} x)^{n_{N1_n}}}{(m_{N1_n} - 1 - n_{N1_n})! n_{N1_n}! (1)_{n_{N1_n}}} \end{aligned} \quad (A.1)$$

and

$$\begin{aligned} f_{|h_{mk}|^2}(x) &= \alpha_{N2_m} e^{-\beta_{N2_m} x} {}_1F_1(m_{N2_m}; 1; \delta_{N2_m} x) \\ &= \alpha_{N2_m} e^{-(\beta_{N2_m} - \delta_{N2_m}) x} \\ &\quad \sum_{n_{N2_m}=0}^{m_{N2_m}-1} \frac{(m_{N2_m} - 1)! (\delta_{N2_m} x)^{n_{N2_m}}}{(m_{N2_m} - 1 - n_{N2_m})! n_{N2_m}! (1)_{n_{N2_m}}} \end{aligned} \quad (A.2)$$

and

$$f_{|h_{ik}|^2}(x) = \frac{1}{\sigma_{BS}^2} e^{-\frac{x}{\sigma_{BS}^2}}, \quad (A.3)$$

where ${}_1F_1(\cdot, \cdot, \cdot)$ is the confluent hypergeometric function, $\alpha_{N2_m} = \frac{(2c_{N2_m} m_{N2_m})^{m_{N2_m}}}{2c_{N2_m} (2c_{N2_m} m_{N2_m} + \Omega_{N2_m})^{m_{N2_m}}}$, $\alpha_{N1_n} = \frac{(2c_{N1_n} m_{N1_n})^{m_{N1_n}}}{2c_{N1_n} (2c_{N1_n} m_{N1_n} + \Omega_{N1_n})^{m_{N1_n}}}$, $\delta_{N1_n} = \frac{\Omega_{N1_n}}{2c_{N1_n} (2c_{N1_n} m_{N1_n} + \Omega_{N1_n})}$, $\delta_{N2_m} = \frac{\Omega_{N2_m}}{2c_{N2_m} (2c_{N2_m} m_{N2_m} + \Omega_{N2_m})}$, $\beta_{N1_n} = \frac{1}{2c_{N1_n}}$ and $\beta_{N2_m} = \frac{1}{2c_{N2_m}}$. $2c_{N1_n}$ and $2c_{N2_m}$ denote the scattered components' average power of the $N1_n$ - U_{N1}^k and of the $N2_m$ - U_{N2}^j links, respectively. Furthermore, Ω_{N1_n} and Ω_{N2_m} are the line-of-sight (LOS) components' average power of the $N1_n$ - U_{N1}^k and $N2_m$ - U_{N2}^j links, respectively, while σ_{BS}^2 is the mean of $|h_{ik}|^2$. Additionally, m_{N1_n} and m_{N2_m} represent the Nakagami fading parameters of the $N1_n$ - U_{N1}^k and $N2_m$ - U_{N2}^j links, respectively.

Using (A.1), P_{OP}^{NGSO1} can be written as

$$\begin{aligned} P_{OP}^{NGSO1} &= \Pr \left(\frac{P_n^o G_{nU_{N1}^k}^t G_{nU_{N1}^k}^r L_{nk}^s |h_{nk}|^2}{\sum_{m=1}^{N'_{S1}} P_m^o G_{mU_{N1}^k}^t G_{mU_{N1}^k}^r L_{mk}^s |h_{mk}|^2 + \sum_{i \in \Phi_{BS}} P_i^o L_{ik}^s |h_{ik}|^2 + \sigma_{N1}^2} \right. \\ &\quad \left. < \phi_{th} \right) \\ &= \Pr \left(|h_{nk}|^2 < \sum_{m=1}^{N'_{S1}} \zeta_m |h_{mk}|^2 + \sum_{i \in \Phi_{BS}} I_{BS_i} |h_{ik}|^2 + S \sigma_{N1}^2 \right), \end{aligned} \quad (A.4)$$

where $\zeta_m = \frac{\phi_{th} P_m^o G_{mU_{N1}^k}^t G_{mU_{N1}^k}^r L_{mk}^s}{P_n^o G_{nU_{N1}^k}^t G_{nU_{N1}^k}^r L_{nk}^s}$, $I_{BS_i} = \frac{\phi_{th} P_i^o L_{ik}^s}{P_n^o G_{nU_{N1}^k}^t G_{nU_{N1}^k}^r L_{nk}^s}$, and $S = \frac{\phi_{th}}{P_n^o G_{nU_{N1}^k}^t G_{nU_{N1}^k}^r L_{nk}^s}$.

Upon denoting $\mu = \sum_{m=1}^{N'_{S1}} \zeta_m |h_{mk}|^2 + \sum_{i \in \Phi_{BS}} I_{BS_i} |h_{ik}|^2 + S \sigma_{N1}^2$,

and $x = |h_{nk}|^2$, $P_{\text{OP}}^{\text{NGSO1}}$ can be formulated as

$$\begin{aligned}
& P_{\text{OP}}^{\text{NGSO1}} \\
&= \int_0^\infty \cdots \int_0^\infty f(|h_{1k}|^2) \cdots f(|h_{N'_{S1}k}|^2) d|h_{1k}|^2 \cdots d|h_{N'_{S1}k}|^2 \\
& \int_0^\infty \cdots \int_0^\infty f(|h_{1k}^t|^2) \cdots f(|h_{N_{\text{BS}k}^t}|^2) d|h_{N_{1k}^t}|^2 \cdots d|h_{N_{\text{BS}k}^t}|^2 \\
& \int_0^u \alpha_{N_{1n}} e^{-(\beta_{N_{1n}} - \delta_{N_{1n}})x} \sum_{n_{N_{1n}}=0}^{m_{N_{1n}}-1} Z_{0N_{1n}} dx \\
&= \int_0^\infty \cdots \int_0^\infty f(|h_{1k}|^2) \cdots f(|h_{N'_{S1}k}|^2) d|h_{1k}|^2 \cdots d|h_{N'_{S1}k}|^2 \\
& \int_0^\infty \cdots \int_0^\infty f(|h_{1k}^t|^2) \cdots f(|h_{N_{\text{BS}k}^t}|^2) d|h_{N_{1k}^t}|^2 \cdots d|h_{N_{\text{BS}k}^t}|^2 \\
& \sum_{n_{N_{1n}}=0}^{m_{N_{1n}}-1} Z_{N_{1n}} \left(1 - e^{-\sum_{m=1}^{N'_{S1}} \zeta_m |h_{mk}|^2} \right. \\
& e^{-\sum_{i \in \phi_{\text{BS}}} I_{\text{BS}_i} |h_{ik}^t|^2} e^{-\sum_{m=1}^{N'_{S1}} \zeta_m |h_{mk}|^2 + \sum_{i \in \phi_{\text{BS}}} I_{\text{BS}_i} |h_{ik}^t|^2 + S\sigma_{N1}^2} \left. \right)^{k_o} \\
& \sum_{k_o=0}^{n_{N_{1n}}} \frac{1}{k_o!} \frac{1}{(\beta_{N_{1n}} - \delta_{N_{1n}})^{-k_o}} \Bigg), \quad (\text{A.5})
\end{aligned}$$

where $Z_{0N_{1n}} = \frac{(m_{N_{1n}}-1)!(\delta_{N_{1n}}x)^{n_{N_{1n}}}}{(m_{N_{1n}}-1-n_{N_{1n}})!n_{N_{1n}}!(1)^{n_{N_{1n}}}}$, and $Z_{N_{1n}} = \frac{\alpha_{N_{1n}}(m_{N_{1n}}-1)!(\delta_{N_{1n}})^{n_{N_{1n}}}}{(m_{N_{1n}}-1-n_{N_{1n}})!(1)^{n_{N_{1n}}}} (\beta_{N_{1n}} - \delta_{N_{1n}})^{n_{N_{1n}}+1}$. $\sum_{k_o=0}^{n_{N_{1n}}} \frac{1}{k_o!} (\beta_{N_{1n}} - \delta_{N_{1n}})^{k_o} \left(\sum_{m=1}^{N'_{S1}} \zeta_m |h_{mk}|^2 + \sum_{i \in \phi_{\text{BS}}} I_{\text{BS}_i} |h_{ik}^t|^2 + S\sigma_{N1}^2 \right)^{k_o}$ can be given by

$$\begin{aligned}
& \sum_{k_o=0}^{n_{N_{1n}}} k_{\beta\delta} \left(\sum_{m=1}^{N'_{S1}} \zeta_m |h_{mk}|^2 + \sum_{i \in \phi_{\text{BS}}} I_{\text{BS}_i} |h_{ik}^t|^2 + S\sigma_{N1}^2 \right)^{k_o} \\
&= \sum_{k_o=0}^{n_{N_{1n}}} \sum_{j_o=0}^{k_o} \sum_{z_o=0}^{j_o} k_{\beta\delta} \binom{k_o}{j_o} \binom{j_o}{z_o} (S\sigma_{N1}^2)^{j_o-z_o} \\
& \sum_{x_m \geq 0, x_1, x_2, \dots, x_{N'_{S1}}} k_{jx} \left(\zeta_1 |h_{1k}|^2 \right)^{x_1} \cdots \left(\zeta_{N'_{S1}} |h_{N'_{S1}k}|^2 \right)^{x_{N'_{S1}}} \\
& \sum_{y_i \geq 0, y_1, y_2, \dots, y_{N_{\text{BS}}}} z_y \left(I_{\text{BS}_1} |h_{1k}^t|^2 \right)^{y_1} \cdots \left(I_{\text{BS}_{N_{\text{BS}}}} |h_{N_{\text{BS}k}^t}|^2 \right)^{y_{N_{\text{BS}}}}, \quad (\text{A.6})
\end{aligned}$$

where $k_{\beta\delta} = \frac{1}{k_o!} (\beta_{N_{1n}} - \delta_{N_{1n}})^{k_o}$, $k_{jx} = \binom{k_o - j_o}{x_1, x_2, \dots, x_{N'_{S1}}}$, and $z_y = \binom{z_o}{y_1, y_2, \dots, y_{N_{\text{BS}}}}$.

Upon relying on [44], and substituting (A.6) into (A.5), we

have

$$\begin{aligned}
P_{\text{OP}}^{\text{NGSO1}} &= \sum_{n_{N_{1n}}=0}^{m_{N_{1n}}-1} \left(Z_{N_{1n}} \prod_{m=1}^{N'_{S1}} \sum_{n_{N_{2m}}=0}^{m_{N_{2m}}-1} Z_{N_{2m}} - \right. \\
& Z_{N_{1n}} e^{-(\beta_{N_{1n}} - \delta_{N_{1n}})S\sigma_{N1}^2} \sum_{k_o=0}^{n_{N_{1n}}} \sum_{j_o=0}^{k_o} \sum_{z_o=0}^{j_o} k_{\beta\delta} \binom{k_o}{j_o} \\
& \binom{j_o}{z_o} (S\sigma_{N1}^2)^{j_o-z_o} \sum_{x_m \geq 0, x_1, x_2, \dots, x_{N'_{S1}}} k_{jx} \prod_{m=1}^{N'_{S1}} (\zeta_m)^{x_m} \\
& \prod_{m=1}^{N'_{S1}} \left(\sum_{n_{N_{2m}}=0}^{m_{N_{2m}}-1} Z_{N_{2m}} (\beta_{N_{2m}} - \delta_{N_{2m}}) (x_m + n_{N_{2m}})! \right. \\
& \left. \left. (\beta_{N_{1n}} - \delta_{N_{1n}}) \zeta_m + (\beta_{N_{2m}} - \delta_{N_{2m}}) \right)^{-x_m - n_{N_{2m}} - 1} \right. \\
& \sum_{y_i \geq 0, y_1, y_2, \dots, y_{N_{\text{BS}}}} z_y \prod_{i=1}^{N_{\text{BS}}} (I_{\text{BS}_i})^{y_i} \prod_{i=1}^{N_{\text{BS}}} \frac{1}{\sigma_{\text{BS}}^2} (y_i)! \\
& \left. \left. \left((\beta_{N_{1n}} - \delta_{N_{1n}}) I_{\text{BS}_i} + \frac{1}{\sigma_{\text{BS}}^2} \right)^{-y_i - 1} \right) \right). \quad (\text{A.7})
\end{aligned}$$

APPENDIX B DERIVATION OF $P_{\text{AOP}}^{\text{BS}}$

Using (A.3), $P_{\text{AOP}}^{\text{BS}}$ can be written as

$$\begin{aligned}
P_{\text{AOP}}^{\text{BS}} &= \Pr(|h_{ik}^t|^2 < S_{abcd}) \\
&= \int_0^\infty \cdots \int_0^\infty f(|h_{1k}|^2) \cdots f(|h_{N'_{S3}k}|^2) d|h_{1k}|^2 \cdots d|h_{N'_{S3}k}|^2 \\
& \int_0^\infty \cdots \int_0^\infty f(|h_{1k}|^2) \cdots f(|h_{N'_{S4}k}|^2) d|h_{1k}|^2 \cdots d|h_{N'_{S4}k}|^2 \\
& \int_0^\infty \cdots \int_0^\infty f(|h_{1k}^t|^2) \cdots f(|h_{N_{\text{BS}k}^t}|^2) \left(1 - e^{-\frac{1}{\sigma_{\text{BS}}^2} S_{abcd}} \right) \\
& d|h_{N_{1k}^t}|^2 \cdots d|h_{N_{\text{BS}k}^t}|^2, \quad (\text{B.1})
\end{aligned}$$

where $A'_n = A_n P_i$, $B'_m = B_m P_i$, $C'_j = C_j P_i$, $D'_i = D_i P_i$, and $S_{abcd} = \sum_{n=1}^{N'_{S3}} A_n |h_{nt}|^2 + \sum_{m=1}^{N'_{S4}} B_m |h_{mt}|^2 + \sum_{j=1, j \neq i}^{N_{\text{BS}}} C_j |h_{jt}|^2 + D_i$.

When $P_i \rightarrow \infty$, then $1 - e^{-\frac{1}{\sigma_{\text{BS}}^2 P_i} S_{abcd}}$ can be given by

$$1 - e^{-\frac{1}{\sigma_{\text{BS}}^2 P_i} S_{abcd}} = \frac{1}{\sigma_{\text{BS}}^2 P_i} S_{abcd}, \quad (\text{B.2})$$

Furthermore, P_{AOP}^{BS} can be finally formulated as

$$\begin{aligned}
P_{AOP}^{BS} = & \frac{1}{\sigma_{BS}^2 P_i} D_i \prod_{n=1}^{N'_{S3}} \sum_{n_{N1_n}=0}^{m_{N1_n}-1} Z_{N1_n} \prod_{m=1}^{N'_{S4}} \sum_{n_{N2_m}=0}^{m_{N2_m}-1} Z_{N2_m} + \\
& \frac{1}{\sigma_{BS}^2 P_i} \prod_{n=1}^{N'_{S3}} \sum_{n_{N1_n}=0}^{m_{N1_n}-1} Z_{N1_n} \prod_{m=1}^{N'_{S4}} \sum_{n_{N2_m}=0}^{m_{N2_m}-1} Z_{N2_m} \prod_{j=1, j \neq i}^{N_{BS}} C'_j \left(\frac{1}{\sigma_{BS}^2} \right)^{-2} + \\
& \frac{1}{\sigma_{BS}^2 P_i} \prod_{n=1}^{N'_{S3}} \sum_{n_{N1_n}=0}^{m_{N1_n}-1} Z_{N1_n} \prod_{m=1}^{N'_{S4}} B'_m \sum_{n_{N2_m}=0}^{m_{N2_m}-1} \frac{Z_{N2_m}}{(\beta_{N2_m} - \delta_{N2_m})} + \\
& \frac{1}{\sigma_{BS}^2 P_i} \prod_{m=1}^{N'_{S4}} \sum_{n_{N2_m}=0}^{m_{N2_m}-1} Z_{N2_m} \prod_{n=1}^{N'_{S3}} A'_n \sum_{n_{N1_n}=0}^{m_{N1_n}-1} Z_{N1_n} (n_{N1_n} + 1)! \\
& (\beta_{N1_n} - \delta_{N1_n})^{-1}. \quad (B.3)
\end{aligned}$$

REFERENCES

- [1] H. He, C. Qin, S. Chen, X. Jiang, J. Yang and L. Hanzo, "Sparse bandit learning based location management for space-ground integrated networks," *IEEE Trans. Veh. Technol.*, vol. 72, no. 8, pp. 10314-10329, Aug. 2023.
- [2] S. Liu, Z. Gao, Y. Wu, D. Kwan Ng, X. Gao, K. Wong, S. Chatzinotas, and B. Ottersten, "LEO satellite constellations for 5G and beyond: How will they reshape vertical domains?" *IEEE Commun. Magazine*, vol. 59, no. 7, pp. 30-36, Jul. 2021.
- [3] Q. Chen, G. Giambene, L. Yang, C. Fan and X. Chen, "Analysis of inter-satellite link paths for LEO mega-constellation networks," *IEEE Trans. Veh. Technol.*, vol. 70, no. 3, pp. 2743-2755, Mar. 2021.
- [4] S. Liu, J. Lin, L. Xu, X. Gao, L. Liu, and L. Jiang, "A dynamic beam shut off algorithm for LEO multibeam satellite constellation network," *IEEE Wireless Commun. Letters*, vol. 9, no. 10, pp. 1730-1733, Oct. 2020.
- [5] M. Sheng, D. Zhou, W. Bai, J. Liu, and J. Li, "6G service coverage with mega satellite constellations," *China Commun.*, vol. 19, no. 1, pp. 64-76, Jan. 2022.
- [6] S. Ji, D. Zhou, M. Sheng, and J. Li, "Mega satellite constellation system optimization: From a network control structure perspective," *IEEE Trans. Wireless Commun.*, vol. 21, no. 2, pp. 913-927, Feb. 2022.
- [7] R. Gopal, and N. BenAmmar, "Framework for unifying 5G and next generation satellite communications," *IEEE Network*, vol. 32, no. 5, pp. 16-24, Sep./Oct. 2018.
- [8] M. Jia, X. Zhang, J. Sun, X. Gu, and Q. Guo, "Intelligent resource management for satellite and terrestrial spectrum shared networking toward B5G," *IEEE Wireless Commun.*, vol. 27, no. 1, pp. 54-61, Feb. 2020.
- [9] Y. Yan, K. An, B. Zhang, W. Zhu, G. Ding, and D. Guo, "Outage-constrained robust multigroup multicast beamforming for satellite-based Internet of Things coexisting with terrestrial networks," *IEEE Internet of Things J.*, vol. 8, no. 10, pp. 8159-8172, May 2021.
- [10] Y. Liang, J. Tan, H. Jia, J. Zhang, and L. Zhao, "Realizing intelligent spectrum management for integrated satellite and terrestrial networks," *J. Commun. Inf. Networks*, vol. 6, no. 1, pp. 32-43, Mar. 2021.
- [11] X. Ding, L. Feng, Y. Zou, and G. Zhang, "Deep learning aided spectrum prediction for satellite communication systems," *IEEE Trans. Veh. Technol.*, vol. 69, no. 12, pp. 16314-16319, Dec. 2020.
- [12] C. Zhang, J. Jin, L. Kuang, C. Jiang, and Y. He, "Blind spot of spectrum awareness techniques in nongeostationary satellite systems," *IEEE Trans. Aerospace Electronic Systems*, vol. 54, no. 6, pp. 3150-3159, Dec. 2018.
- [13] X. Liu, K. Lam, F. Li, J. Zhao, L. Wang, and T. Durrani, "Spectrum sharing for 6G integrated satellite-terrestrial communication networks based on NOMA and CR," *IEEE Network*, vol. 35, no. 4, pp. 28-34, Jul./Aug. 2021.
- [14] J. Hu, G. Li, D. Bian, L. Gou, and C. Wang, "Optimal power control for cognitive LEO constellation with terrestrial networks," *IEEE Commun. Letters*, vol. 24, no. 3, pp. 622-625, Mar. 2020.
- [15] H. Baek, and J. Lim, "Spectrum sharing for coexistence of fixed satellite services and frequency hopping tactical data link," *IEEE J. Sel. Areas Commun.*, vol. 34, no. 10, pp. 2642-2649, Oct. 2016.
- [16] Y. Sagduyu, Y. Shi, A. MacKenzie, and Y. Hou, "Regret minimization for primary/secondary access to satellite resources with cognitive interference," *IEEE Trans. Wireless Commun.*, vol. 17, no. 5, pp. 3512-3523, May 2018.
- [17] C. Zhang, C. Jiang, L. Kuang, J. Jin, Y. He, and Z. Han, "Spatial spectrum sharing for satellite and terrestrial communication networks," *IEEE Trans. Aerospace Electronic Systems*, vol. 55, no. 3, pp. 1075-1089, Jun. 2019.
- [18] H. Zhang, C. Jiang, J. Wang, L. Wang, Y. Ren and L. Hanzo, "Multicast beamforming optimization in cloud-based heterogeneous terrestrial and satellite networks," *IEEE Trans. Veh. Technol.*, vol. 69, no. 2, pp. 1766-1776, Feb. 2020.
- [19] M. Jia, X. Zhang, X. Gu, Q. Guo, Y. Li, and P. Lin, "Interbeam interference constrained resource allocation for shared spectrum multibeam satellite communication systems," *IEEE Internet of Things J.*, vol. 6, no. 4, pp. 6052-6059, Aug. 2019.
- [20] Y. Zhang, H. Zhang, H. Zhou, K. Long and G. Karagiannidis, "Resource allocation in terrestrial-satellite-based next generation multiple access networks with interference cooperation," *IEEE J. Sel. Areas Commun.*, vol. 40, no. 4, pp. 1210-1221, Apr. 2022.
- [21] P. Gu, R. Li, C. Hua, and R. Tafazolli, "Dynamic cooperative spectrum sharing in a multi-beam LEO-GEO co-existing satellite system," *IEEE Trans. Wireless Commun.*, vol. 21, no. 2, pp. 1170-1182, Feb. 2022.
- [22] C. Braun, A. M. Voicu, L. Simic and P. Mahonen, "Should we worry about interference in emerging dense NGSO satellite constellations?" in *Proc. IEEE International Symposium on Dynamic Spectrum Access Networks (DySPAN)*, 2019, pp. 1-10.
- [23] Y. He, Y. Li and H. Yin, "Co-frequency interference analysis and avoidance between NGSO constellations: Challenges, techniques, and trends," *China Commun.*, vol. 20, no. 7, pp. 1-14, July 2023.
- [24] X. Zhang, B. Zhang, K. An, G. Zheng, S. Chatzinotas, and D. Guo, "Stochastic geometry-based analysis of cache-enabled hybrid satellite-aerial-terrestrial networks with non-orthogonal multiple access," *IEEE Trans. Wireless Commun.*, vol. 21, no. 2, pp. 1272-1287, Feb. 2022.
- [25] J. Sun, F. Liu, H. Wang, M. Ahmed, Y. Li and M. Liu, "Efficient VNF placement for Poisson arrived traffic," *IEEE Trans. Network Service Management*, vol. 18, no. 4, pp. 4277-4293, Dec. 2021.
- [26] I. del Portillo, B. Cameron, and E. Crawley, "A technical comparison of three low earth orbit satellite constellation systems to provide global broadband," *Acta Astronautica*, vol. 159, pp. 123-135, Jun. 2019.
- [27] M. A. Velasquez et al., "Precoding in multibeam satellite communications: Present and future challenges," *IEEE Wireless Commun.*, vol. 23, no. 6, pp. 88-95, Dec. 2016.
- [28] M. Jia, X. Zhang, X. Gu, Q. Guo, Y. Li and P. Lin, "Interbeam interference constrained resource allocation for shared spectrum multibeam satellite communication systems," *IEEE Internet Things J.*, vol. 6, no. 4, pp. 6052-6059, Aug. 2019.
- [29] T. Humphreys, P. Iannucci, Z. Komodromos, and A. Graff, "Signal structure of the Starlink Ku-band downlink," available online: <https://arxiv.org/abs/2210.11578v1>.
- [30] S. R. Pratt, R. A. Raines, C. E. Fossa and M. A. Temple, "An operational and performance overview of the IRIDIUM low earth orbit satellite system," *IEEE Commun. Surveys*, vol. 2, no. 2, pp. 2-10, Second Quarter 1999.
- [31] C. Liu, X. Liu, D. W. K. Ng, and J. Yuan, "Deep residual learning for channel estimation in intelligent reflecting surface-assisted multi-user communications," *IEEE Trans. Wireless Commun.*, vol. 21, no. 2, pp. 898-912, Feb. 2022.
- [32] H. Mosavat-Jahromi, Y. Li, L. Cai, and J. Pan, "Prediction and modeling of spectrum occupancy for dynamic spectrum access systems," *IEEE Trans. Cog. Commun. Netw.*, vol. 7, no. 3, pp. 715-728, Sept. 2021.
- [33] X. Huang, Y. Li, Y. Gao, and X. Tang, "Q-learning-based spectrum access for multimedia transmission over cognitive radio networks," *IEEE Trans. Cog. Commun. Netw.*, vol. 7, no. 1, pp. 110-119, Mar. 2021.
- [34] H. Li, X. Ding, Y. Yang, Z. Xie, and G. Zhang, "Online spectrum prediction with adaptive threshold quantization," *IEEE Access*, vol. 7, pp. 174325-174334, 2019.
- [35] B. Yang, X. Cao, J. Basseby, X. Li and L. Qian, "Computation offloading in multi-access edge computing: A multi-task learning approach," *IEEE Trans. Mobile Computing*, vol. 20, no. 9, pp. 2745-2762, Sept. 2021.
- [36] X. Cao et al., "Edge-assisted multi-layer offloading optimization of LEO satellite-terrestrial integrated networks," *IEEE J. Sel. Areas Commun.*, vol. 41, no. 2, pp. 381-398, Feb. 2023.

- [37] C. Kosta, B. Hunt, A. U. Qaddus and R. Tafazolli, "On interference avoidance through inter-cell interference coordination (ICIC) based on OFDMA mobile systems," *IEEE Commun. Surveys Tutorials*, vol. 15, no. 3, pp. 973-995, Third Quarter 2013.
- [38] Z. Wang, Y. Zhou, Y. Shi and W. Zhuang, "Interference management for over-the-air federated learning in multi-cell wireless networks," *IEEE J. Sel. Areas Commun.*, vol. 40, no. 8, pp. 2361-2377, Aug. 2022.
- [39] J. Ye, S. Dang, B. Shihada, and M. Alouini, "Space-air-ground integrated networks: Outage performance analysis," *IEEE Trans. Wireless Commun.*, vol. 19, no. 12, pp. 7897-7912, Dec. 2020.
- [40] H. Jia, Z. Ni, C. Jiang, L. Kuang, and J. Lu, "Uplink interference and performance analysis for megasatellite constellation," *IEEE Internet Things J.*, vol. 9, no. 6, pp. 4318-4329, Mar. 2022.
- [41] F. Gers, J. Schmidhuber and F. Cummins, "Learning to forget: Continual prediction with LSTM," *Neural Comput.*, vol. 12, no. 10, pp. 2451-2471, 2000.
- [42] X. Ding, Q. Lv, Y. Zou and G. Zhang, "Spectrum prediction for satellite based spectrum-sensing systems using deep learning," in *Proc. IEEE Global Communi. Conf. (GLOBECOM)*, Rio de Janeiro, Brazil, 2022, pp. 3472-3477.
- [43] M. Gong, J. Liu, A. K. Qin, K. Zhao and K. C. Tan, "Evolving deep neural networks via cooperative coevolution with backpropagation," *IEEE Trans. Neural Netw. Learning Systems*, vol. 32, no. 1, pp. 420-434, Jan. 2021.
- [44] I. S. Gradshteyn, and I. M. Ryzhik, "Table of Integrals, Series, and Products," New York, Academic Press, 2007.